Quaternary Science Advances 10 (2023) 100081

Contents lists available at ScienceDirect

Quaternary Science Advances

journal homepage: www.sciencedirect.com/journal/quaternary-science-advances

Relationship between depositional environments and preservabilities of Holocene tsunami deposits on the Hidaka coast, Hokkaido, Japan

Ryo Nakanishi [a,b,*], Juichiro Ashi [a,b], Yosuke Miyairi [a], Yusuke Yokoyama [a,c,d,e,f]

[a] Atmosphere and Ocean Research Institute, The University of Tokyo, Kashiwa, 277-8564, Japan
[b] Graduate School of Frontier Sciences, The University of Tokyo, Kashiwa, 277-8561, Japan
[c] Department of Earth and Planetary Sciences, Graduate School of Science, The University of Tokyo, Japan
[d] Graduate Program on Environmental Science, Graduate School of Arts and Sciences, The University of Tokyo, Japan
[e] Japan Agency for Marine-Earth Science and Technology (JAMSTEC), Japan
[f] Research School of Physics, The Australian National University, Canberra, ACT0200, Australia

ARTICLE INFO

Keywords:
Sea level index points
Tsunami deposits
Diatom
Depositional environment
Preservation potential

ABSTRACT

Rising sea levels and associated coastal topography changes are expected to increase coastal vulnerability to tsunamis. Reliable records of the periodicity of the most damaging tsunamis, with recurrence intervals of several centuries, are often incomplete. To understand the likelihood of coastal disasters that would be worsened by sea-level rise, as well as their possible occurrence leading to the actual extent of inland inundation, it is useful to examine the geological record of the mid-Holocene highstand periods to supplement the written archives. However, the formation and preservation potential of event layers depends heavily on the depositional environment resulting from coastal evolutions. This study attempted to reconstruct the depositional environment changes using diatom and chemical analyses on the Hidaka coast of Hokkaido, Japan, to examine the preservation of event layer archives.

Following field investigations, we found three sand layers formed by extreme waves from field investigations. The relationship between the depositional environment and the timing of the event layer formation over the past 7000 years along the central Hidaka coast indicates that supratidal to freshwater marsh environments are the most suitable for preserving tsunami deposits in this region. Since sand layers in the distant areas from wave sources were not well preserved in upland (as at elevations above marsh environment) and saltmarsh environments, the time windows of preservation were very limited depending on the depositional environments with relative sea-level changes. On the other hand, in areas closer to the Kuril Trench, sand layers were preserved not very sensitive to the depositional environment, suggesting that the event archive length is related to the magnitude of tsunamis.

1. Introduction

Sea-level rise is expected to exacerbate many future coastal disasters (Dura et al., 2021). In particular, some studies have indicated that the impact of extreme events, such as storm surges and tsunamis, is greatly affected by relative sea-level (RSL) changes (Dura et al., 2011, 2015, 2016; Brill et al., 2016; Kelsey et al., 2015; Yokoyama et al., 2019a; Nakanishi et al., 2020a) . For tsunamis, a recent simulation predicts that sea-level rise will cause significant damage to coastal plains impacted by tsunamis, even in places that are globally distant from the usual origins of tsunami waves (Dura et al., 2021).

It is known that RSL was higher than today in the mid-Holocene 'far-field', remote from the sites of former glaciation and subsequent isostatic rebound (Yokoyama et al., 2012, 2019a; Yokoyama and Purcell, 2021). This far-field elevation is known as the mid-Holocene sea--level highstand (HHS). The HHS period is considered to be a useful model of a contemporary near future affected by sea-level rise; the identification of coastal disasters that occurred during this period will therefore help with the assessment of future risk. It will be possible to determine whether the sea-level rise that produced the HHS caused more severe tsunami impacts at sites distant from the tsunami source, by examining the geological record.

Whether distinctive deposits of sand and other debris that are often caused by tsunamis and storm surges—deposits referred to as event

* Corresponding author. Atmosphere and Ocean Research Institute, The University of Tokyo, Kashiwa, 277-8564, Japan.
E-mail address: r-nakanishi@aori.u-tokyo.ac.jp (R. Nakanishi).

https://doi.org/10.1016/j.qsa.2023.100081
Received 16 September 2022; Received in revised form 31 January 2023; Accepted 10 February 2023
Available online 11 February 2023

layers in this study—can accurately inform us of the occurrence, wave height, and run-up of such inundations depends both on the conditions at the time, such as sedimentation rate, and on subsequent conditions, such as the biogenous soil mixing rate, whereby a deposit once formed may be erased (Wheatcroft, 1990; Leorri et al., 2009; Spiske et al., 2013). The potential for event layer formation at any given location is assumed to depend on the distance from the shoreline, the height of the local ground above actual sea level at the time (including whether the tide was high or low), the height of any beach ridge, and also wave heights. Therefore, the presence or absence of event layers does not correspond faithfully to the actual history of local coastal inundations in every case. To better interpret the geological traces of past coastal inundations due to tsunamis or storms, it is necessary to identify all the potentially confounding influences of the local geology and topography to understand the interaction of the coastal evolution and its depositional environment with the effects of any difference in RSL at the time of any past inundation events (Nakanishi et al., 2022a).

Coastal marshes distributed between beach ridges are considered suitable for detecting event layers such as tsunami or storm deposits (e.g., Scileppi and Donnelly, 2007; Spiske et al., 2013). Even "coastal marsh" in one word, it shows a diversity of depositional environments (e.g., freshwater marsh and saltmarsh), and the degree to which they preserve past geological traces is also thought to be variable (Leorri et al., 2009). Since there are few examples of studies on the interaction of coastal evolution processes with RSL changes and the formation of tsunami deposits (Chagué et al., 2020; Fujiwara et al., 2020, 2022; Nakanishi et al., 2020a, 2022a), it is still not fully clear what kind of depositional environment within coastal marshes is most suitable for the preservation of an accurate record of past inundations, including those that occurred in the time of the HHS.

This study focused on areas far from the tsunami wave source and conducted a field survey along the Hidaka coast of Hokkaido to identify the event layers and the depositional environment evolution. Inundation traces in these distant areas are suitable for assessing the effects of the depositional environment on preservation. The relationship between the age of the event layers and the depositional environment was discussed by organizing the added geological data and previous studies along the Hidaka coast. Our findings reveal the environment in which event layers are most likely to be formed and preserved, and thus furnish information that will help to understand the true history of low-frequency inundations and their future inundation potential under conditions of future sea-level rise, more generally.

2. Previous studies

The southern Kuril Trench is a subduction zone east of Hokkaido where, based on reliable local records of the earthquakes of the last 200 years (the earlier record is less reliable), Mw~8 earthquakes have occurred at intervals of 50–100 years (Satake, 2015). For the past several thousand years, some studies related to tsunami deposits in eastern Hokkaido have revealed the occurrence of tsunamis generated by earthquakes of much larger magnitude than any southern Kuril Trench earthquake observed over the last 200 years (Nanayama et al., 2003; Sawai, 2020). The recurrence intervals of these large tsunamis were estimated to be several hundred years (Sawai et al., 2009; Ishizawa et al., 2017); the most recent is believed, based on numerical simulation of the tsunami deposits in eastern Hokkaido, to have originated from the 17th-century earthquake of magnitude Mw 8.8 (Ioki and Tanioka, 2016). On the other hand, the observed heights of tsunami waves impacting the Hidaka coast over the last 200 years have not significantly exceeded 2 m (Nakanishi et al., 2020a), because the Hidaka coast does not directly face the southern Kuril Trench (Fig. 1). However, the geological record suggests that larger tsunamis generated by cyclical earthquakes with recurrence intervals of several hundred years have

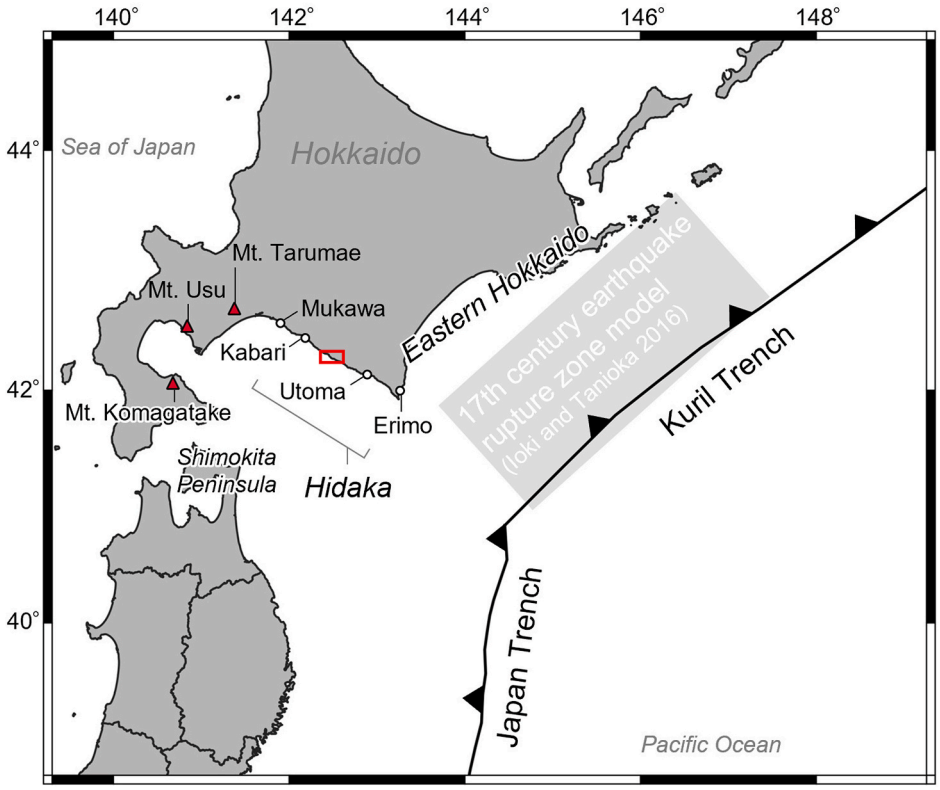

Fig. 1. Map of northern Japan. The red boxes indicate the range of Fig. 2a. Geological survey sites in Hidaka, Hokkaido are shown. A gray box indicates the 17th-century earthquake model (Ioki and Tanioka, 2016). (For interpretation of the references to color in this figure legend, the reader is referred to the Web version of this article.)

reached the Hidaka coast (Nakanishi et al., 2020a, 2022a). These tsunami deposit surveys have been conducted from Erimo westward to Shizunai (Nakanishi et al., 2020a, 2022a, 2022b); numerical simulations and date-range correlations carried out on the deposits from Erimo westward to the Hidaka coast at Shizunai have revealed the presence of several deposits formed by larger tsunamis that may have originated from the Kuril Trench (Nakanishi et al., 2022a; Nakanishi and Ashi, 2022). However, the sedimentary archive on the Hidaka coast is fragmented. For that reason, a reliable, long-term tsunami history including the time of the HHS has not fully been established there.

3. Geological setting

The Harutachi area, on the Hidaka coast northwest of Erimo Cape, has a shallow bay topography extending for ~1.5 km with peat and floodplain deposits behind a 5–8 m high beach berm (Fig. 2). The NE–SW Otoe syncline and the Harutachi anticlinal fault are distributed in Harutachi (Wada et al., 1992). The natural course of the local Fuji River, still evident in an aerial photograph taken in 1948 (the river has since been straightened), reflects the known fold structure of the underlying geology (Fig. 2b). The overall geology of our study area is classified as Neogene Miocene. From southwest to northeast, it consists of conglomerate, alternating beds of sandstone and tuffaceous siltstone, and hard shale (Wada et al., 1992). The shoreline is distributed along with the anticlinal structure, and the basement rocks form the outcrops visible in the 1948 aerial photograph that also shows the old course of the Fuji River (Fig. 2b). Marine terraces formed during the marine isotope stage (MIS) 7 are located at 85–90 m above the present-day sea-level (asl; Koike and Machida, 2001). The MIS 5e terraces are not distributed nearby, but the height of the surrounding coastal area is 45–55 m asl. The uplift rate considering the global sea-level change in the MIS 5e time scale is 0.36–0.46 mm/yr. The rate of local crustal deformation has been measured closely, over the last few decades, with the aid of the global navigation satellite system (GNSS) and level surveys, and is considered to be minimal (Kato, 1983; Murakami and Ozawa, 2004).

The Holocene RSL models around Hokkaido have been reported by glacial-isostatic adjustment (GIA) modeling and sea-level index points (SLIPs), which are derived from the geological traces of tidal levels (Yokoyama et al., 2012). The RSL in the Harutachi area at 6000 years ago is estimated to be 0.5–2.5 m asl (Okuno et al., 2014). The coast of Harutachi is wave-dominated and microtidal; the mean higher high water (MHHW) and highest astronomical tide (HAT) datums are mean sea level (MSL) + 0.4 m and +0.6 m, respectively; these figures are derived from the nearest tide station data for the years 2016–2018 (Japan Metrological Agency: https://www.jma.go.jp/jma/indexe.html [accessed June 2020]).

4. Method

4.1. Field survey

We conducted field surveys along two survey lines (Line A along the shoreline and Line B perpendicular to the shoreline), with samples taken from handy borings and observations of outcrops. Core sampling and subsequent stratigraphic observations (e.g., colors, grain sizes, thicknesses, bedforms) were conducted using a hand corer (7 cm diameter) and a hand geoslicer (a 7 cm width by 1 m length; Takada et al., 2002).

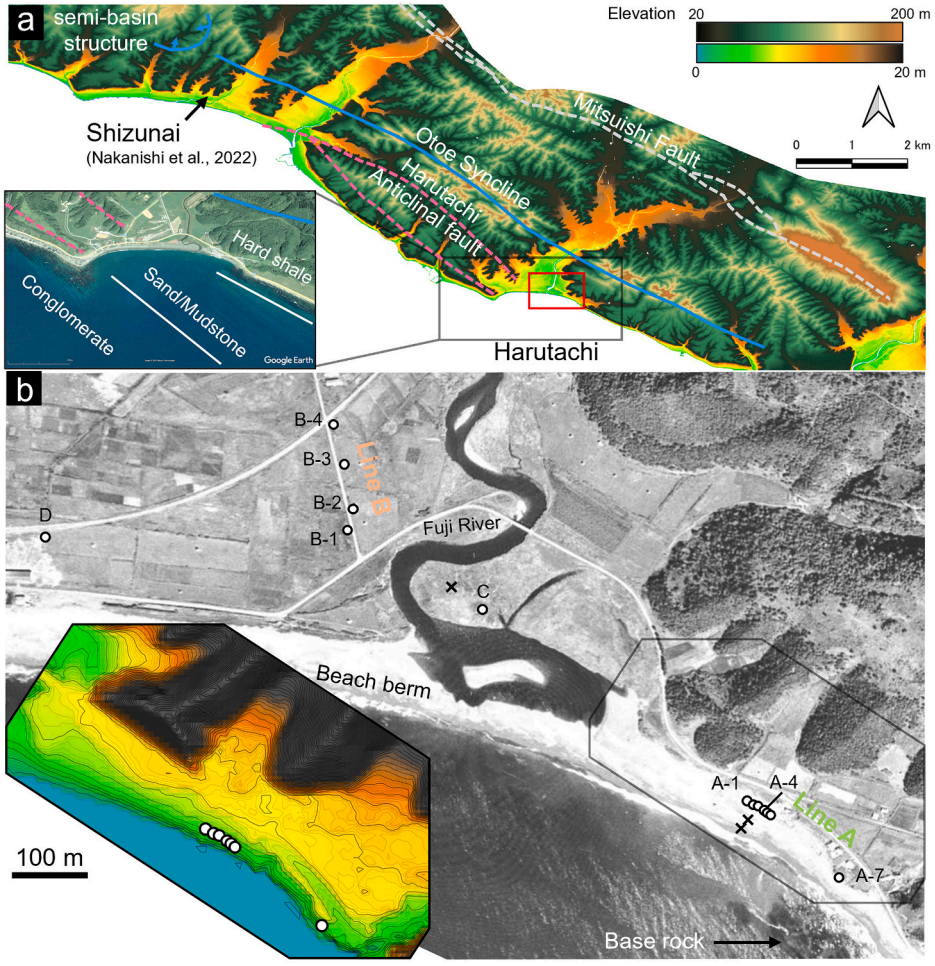

Fig. 2. Topographic map and aerial photograph in the study area. (a) 5 m-grid digital elevation model data on the central Hidaka coast. Blue line indicates syncline (Wada et al., 1992). Dotted lines show faults. The insert shows an aerial view of the vernal stand and the formation of the basement rock delineated by the dotted line (Wada et al., 1992). The red square indicates the area of Fig. 2b. (b) Survey lines and site are shown in an aerial photograph taken in 1948 (the geospatial information authority of Japan: https://mapps.gsi.go.jp/). The x marks indicate the point where the reference sample was taken. The insert shows the close-up map of the slope failure topographies. Elevation legend is the same as in Fig. 2a. (For interpretation of the references to color in this figure legend, the reader is referred to the Web version of this article.)

Samples obtained with the geoslicer were sampled in plastic cases or bags. The sediment description was based on the modified Tröels-Smith (1955) system (Nelson, 2015). The coordinates and elevations of the coring sites were obtained by GNSS survey with an error of within 1 cm with multi-band receivers (ZED-F9P U-blox), comparing the continuous observation data of Geospatial Information Authority of Japan's electronic reference points at the 'Mitsuishi' station.

4.2. Determination of new SLIPs

To clarify the Holocene SLIPs in this area, we used diatom and element analysis. Interpretation of paleo-sea levels from diatom and elemental analysis is based on Nakanishi et al. (2022a). Diatom assemblage analysis was conducted to reconstruct the depositional environment, such as its salinity and hydraulic conditions. Salinity was determined qualitatively based on indicator species (Sawai and Nagumo, 2003; Sawai et al., 2004a; Chiba and Sawai, 2014; Zong and Sawai, 2015). Marine sediments are known to have total sulfur concentrations of >0.3% and a ratio of total organic carbon to total sulfur (TOC/TS) of <10 (Berner and Raiswell, 1984; Sato, 2001).

4.2.1. Diatom analysis

Subsamples of 1 cm thickness were taken from cores at several centimeter intervals, and they were treated with 15% hydrogen peroxide for organic matter, after which 10 cc was dropped into a cover glass and sealed with Pleurax medium (Mountmedia, Wako). Slides were observed by optical microscope (1000× magnification) and counted until 300 diatom valves were observed. Species identification was based on global (Krammer et al., 1986; 1988, 1991a, b; Witkowski et al., 2000) and Japanese catalogs (Sawai and Nagumo, 2003; Watanabe et al., 2005; Kihara et al., 2015; Chiba et al., 2018). Diatom species were classified based on salinity (marine, marine–brackish, brackish, brackish–freshwater, and freshwater) and life form (planktonic, epontic, and benthic), followed by ecological references (Denys, 1991; Vos and de Wolf, 1993; Dam et al., 1994; Chiba and Sawai, 2014; Zong and Sawai, 2015). Neogene diatoms in the central Hidaka coast were reported by Sagayama et al. (1992). We excluded the Neogene species based on the list of Sagayama et al. (1992) from the assemblage analysis because the allochthonous contribution of older, potential fossil species to the water column as a result of erosion of still older deposits may lead to a misreading of the depositional environment at the dates of interest (Chiba et al., 2021). We only used species that constituted more than 3% of the total as significantly present for the subsequent diatom assemblage analysis while rejecting the less common species.

4.2.2. Carbon and sulfur element analysis

Subsamples of 1 cm thickness were taken from cores at several centimeter intervals, and their carbonates were removed with 1 M HCl. They were dried in an oven at 50 °C for 12 h and crushed with a mortar and pestle. Then 20–30 mg powder samples were wrapped in silver cups and measured by a combustion elemental analyzer (Vario EL cube, Elementar).

4.3. Loss on ignition (LOI) and grain size analysis

LOI is known to be a proxy for organic carbon content (Bojko and Kabała, 2014). It was used in combination with sieving to determine the composition of the clastic material. Sand and mud samples were taken from each core in 2–3 cm depth increments (or in 5–10 cm depth increments where a stratigraphic change had not occurred) and were weighed as W_{wet}, dried at 105 °C for 12 h, and re-weighed as W_{105}. The moisture content was calculated by taking the ratio W_{105}/W_{wet}. The dried samples were heated in a muffle furnace up to 550 °C for 5 h and weighed once more as W_{550}. The LOI was calculated by taking the ratio of W_{105} to W_{550}. The ignition samples were divided into sand and mud compartments by a 60 μm sieve. The LOI, mud, and sand weights were normalized and expressed so that the total of these weights was 100%.

Grain size analysis of the sand layers was performed to estimate their source. This work included the collection of current beach sands as a control. For the potential event sands, bulk samples were pretreated with hydrogen peroxide to disperse and decompose organic matter. The treated samples were dried and sieved to 1/2 phi intervals and weighed. Vertical changes in the grain size of sand layers were exhibited every 1 cm.

4.4. X-ray computer tomography (CT)

The CT images are useful for understanding fine sedimentary structures based on density differences between successive layers. The samples were imaged in plastic cases, with a slice width of 0.5 mm, by a medical CT scanner (Aquilion PRIME Focus Edition, Canon Medical Systems Corporation) at the Kochi Core Center. The resulting CT values are shown as median per slice.

4.5. X-ray fluorescence core scanner

The chemical composition of the cores was also determined along their length to provide further information about the source. The samples, in plastic cases, were analyzed by an X-ray fluorescence core scanner (ITRAX, COX Analytical Systems) at the Kochi Core Center. The measurement conditions were as follows: step size of 1 mm, exposure time of 25 s with settings of 50 mA and 60 kV, using a molybdenum anode (Mo) tube. Mo ratios of incoherent and coherent scattering (inc/coh) measured during the analysis were used as a proxy for H, C, N, and O as organic material and water, as reported in (Woodward and Gadd, 2019) and in previous studies (Chagué et al., 2020). The results were expressed as counts per second (cps); if the mean squared error was more than 5, the reading was excluded from the dataset to be plotted.

4.6. X-ray diffraction (XRD)

Mineral composition analysis of sand and mud samples was performed to determine the source of the sediments. As a pretreatment, bulk sand and mud samples were dried and powdered with a mortar and pestle. The powdered samples were measured by an XRD analyzer (D2 PHASER, Bruker). The analysis conditions were set at 30 kV, 10 mA, 0.02 steps for 1 s, and a 2θ registration range from 5° to 65°.

4.7. Radiocarbon dating

Wood fragments and plant leaves picked from core samples were pretreated with 1 M HCl for 1 h to remove calcium carbonate. The CO_2 obtained by heating these samples was recovered and graphitized using Fe powder in a hydrogen atmosphere (Yokoyama et al., 2007). The ^{14}C dating was performed, using single-stage accelerator mass spectrometry at the Atmosphere and Ocean Research Institute (Yokoyama et al., 2019b). The ^{14}C ages were calibrated to calendar ages using the OxCal 4.4 (Bronk Ramsey, 2017) with the IntCal20 dataset (Reimer et al., 2020). The depositional ages of the sand layers were constrained by a sequence model (Bronk Ramsey, 2008).

5. Results

5.1. Stratigraphy

In our study area, seven volcanic ash layers were identified by mineralogical and chemical analysis (Nakanishi et al., 2020b). From bottom to top, two Komagatake volcano tephras, 400 BC Tarumae volcano-c2 tephra (Ta-c2), 946 AD Baegdusan volcano-Tomakomai tephra (B–Tm), and three volcanic ash layers could be traced to 17th-century eruptions (1694 AD Komagatake-c2 tephra, 1667 AD Tarumae-b tephra, 1663 AD Usu-b tephra: Us-b) (Fig. 3). Because the ^{14}C dating obtained from the peat layer between two Komagatake tephras showed 6.3 kyr cal BP (Table 1), these tephras are considered to be the

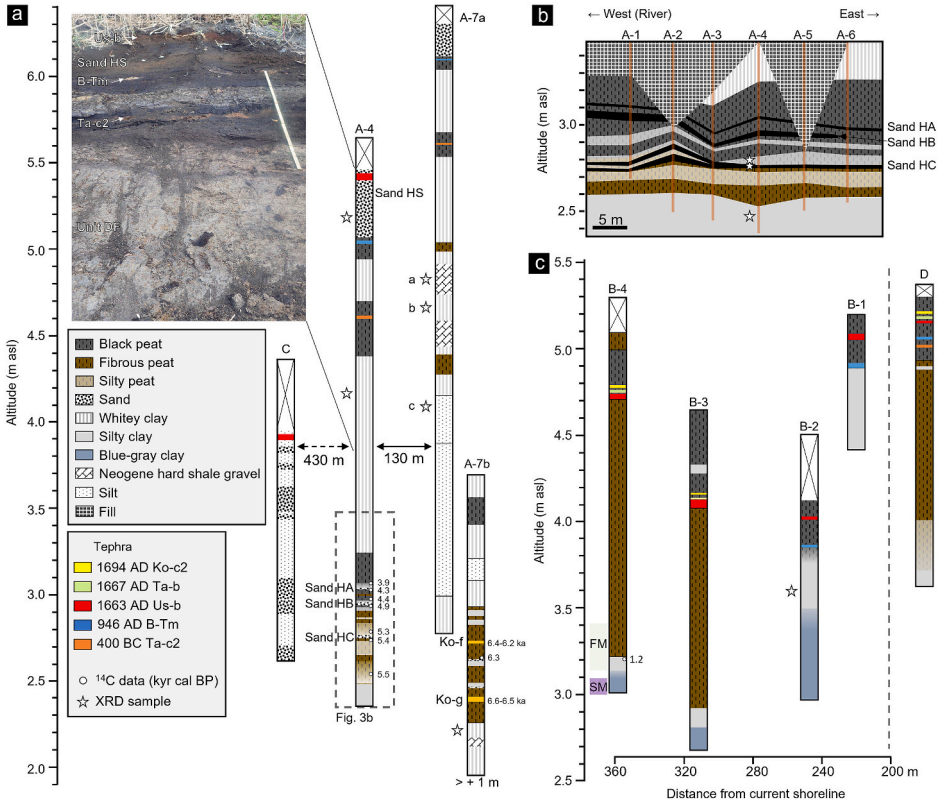

Fig. 3. The sediment stratigraphy on the survey lines. a: The sediment stratigraphy on Line A and Site C. The photograph shows the outcrop in Site A-4. A-7a and A-7b are different outcrop faces in the same Site A-7. b: Detailed lithological cross section based on core observations on Line A. c: The sediment stratigraphy on Line B and Site D.

Komagatake-f tephra (Ko-f, deposited in 6.4–6.2 kyr cal BP: Okuno et al., 1999) and Komagatake-g tephra (Ko-g, deposited in 6.6–6.5 kyr cal BP: Chen et al., 2022), which are known to be regionally widespread deposits (Furukawa and Nanayama, 2006; Nakamura, 2016). Since the area where Ko-f tephra was identified was hitherto limited to the area around Mt. Komagatake (Furukawa and Nanayama, 2006), the discovery of this tephra on the Hidaka coast indicates that it is regionally widespread tephra.

The stratigraphy of Line A consists, from bottom to top, of white silty clay ("Th1, As3" or "As4"), an alternation of fibrous peat ("Th2, As1, Ag1") and white silty peat ("Th1, Ag2, Ga1"), black peat ("Sh2, As2") and white clay ("As4") above ~3.0 m asl, and poorly sorted sand ("Sh1, Ga-m3": called Sand HS) (Fig. 3). Three sand layers each of a few centimeters in thickness are also interbedded in the fibrous or silty peat. From the top, these sand layers are named Sand HA, Sand HB, and Sand HC. In the A-7 site, the A-7a outcrop consists of the peat layers with white clay ("As4"), which includes hard shale gravels, and ("Sh3, Th1") interbedded with silt ("Sh1, As1, Ag2"). The A-7b outcrop (2–3.5 m asl) consists of grayish white clay ("As4") with hard shale gravels, fibrous peat ("Sh1, Th3"), and grayish-white clayey silt ("As1, Ag3"). The fine-grained sand layers in fibrous peat between Ko-f and Ko-g tephras are less than 1 cm thick.

In Line B, the peat layer is more than 2 m thick, and changes from fibrous peat ("Tl2, Th2" or "Sh1,Tl1, Th2") below to black peat ("Sh3, Th1") above (Fig. 3). Blue-gray clay ("As4") underlay the fibrous peat layer with a shape boundary, and the blue-gray clay layer grows thicker

Table 1
The ^{14}C dating results and the depositional ages of the event layers in Harutachi.

Sample name	Site	Depth (cm)	Material	^{14}C age	Error	Modelled age (1σ) from	Modelled age (1σ) to	Modelled age (2σ) from	Modelled age (2σ) to	Mean	Lab number
828Au	A-4	382	Plant fragment	3609	±25	3974	3886	4065	3841	3928	YAUT-047731
Sand HA	A-4	385				4270	3992	4350	3911	4131	
828Al	A-4	387	Plant fragment	3944	±25	4373	4293	4418	4252	4333	YAUT-047732
828Bu	A-4	391	Plant fragment	3914	±27	4418	4354	4503	4297	4380	YAUT-047736
Sand HB	A-4	394				4840	4496	4890	4366	4632	
828Bl	A-4	396	Plant fragment	4314	±28	4955	4841	4961	4836	4884	YAUT-047737
828Cu	A-4	405	Plant fragment	4642	±26	5402	5310	5449	5138	5336	YAUT-047738
Sand HC	A-4	412				5433	5353	5457	5314	5381	
828Cl	A-4	408	Plant fragment	4638	±26	5451	5409	5470	5374	5425	YAUT-047739
828_Cb5-6	A-4	415	Wood fragment	4763	±31	5560	5470	5583	5462	5517	YAUT-071729
Sample name	Site	Depth (cm)	Material	^{14}C age	Error	Calibrated age (1σ) from	Calibrated age (1σ) to	Calibrated age (2σ) from	Calibrated age (2σ) to	Mean	Lab number
872_200 cm	B-2	200	Wood fragment	1292	±21	1275	1179	1285	1176	1228	YAUT-071731
947_30	A-7	102	Wood fragment	5501	±30	6386	6279	6393	6212	6302	YAUT-071732

toward the southern end of Line B. Near the Fuji River (B-1 and B-2), the blue-gray clay layer underlays B–Tm tephra without fibrous peats.

In Site C, where an outcrop near the river mouth was observed, the stratigraphy was an alternation of silt ("Ag3, As1") and sand layers below Us-b (Fig. 3). The upper sand layers are clear basal contacts with silt, while the lower sand layers tended to be fine-grained and have unclear basal contacts. Site D is located to the west of Line B. The five volcanic ash layers were identified in black peats ("Sh3, Th1": Fig. 3). The fibrous peat ("Sh1, Th3") of ~1 m thickness was deposited below the Ta-c2 tephra, which changed to a silty peat ("Th2, As1, Ag1") and a silty clay layer ("Th1, As1, Ag2") at the bottom.

5.2. Diatom and elemental analyses

Site A-4. The sediments of Site A-4 were divided into five units based on the similarity of diatom assemblages (Fig. 4). Unit SM (meaning 'Saltmarsh') consists of silty clay and is dominated by *Navicula peregrina* and *Tabularia fasciculata*. The silty fibrous peat layer (~2.5 m asl) includes *Staurosira* and *Pseudostaurosira* spp., which are dominant in enclosed brackish to fresh waters (Stabell, 1985; Ludikova et al., 2020). Unit ST (meaning 'Supratidal') consists of the silty fibrous layer and is dominated by benthic brackish species, such as *Diploneis pseudovalis*, brackish-fresh water species, such as *Cosmioneis pusilla*, and Neogene diatoms. Unit FM (meaning 'Freshwater marsh') consists of fibrous or black peats; the dominant species are freshwater benthic species, such as *Pinnularia* spp., *Diploneis* spp., and *Hantzschia amphioxys*. This unit was

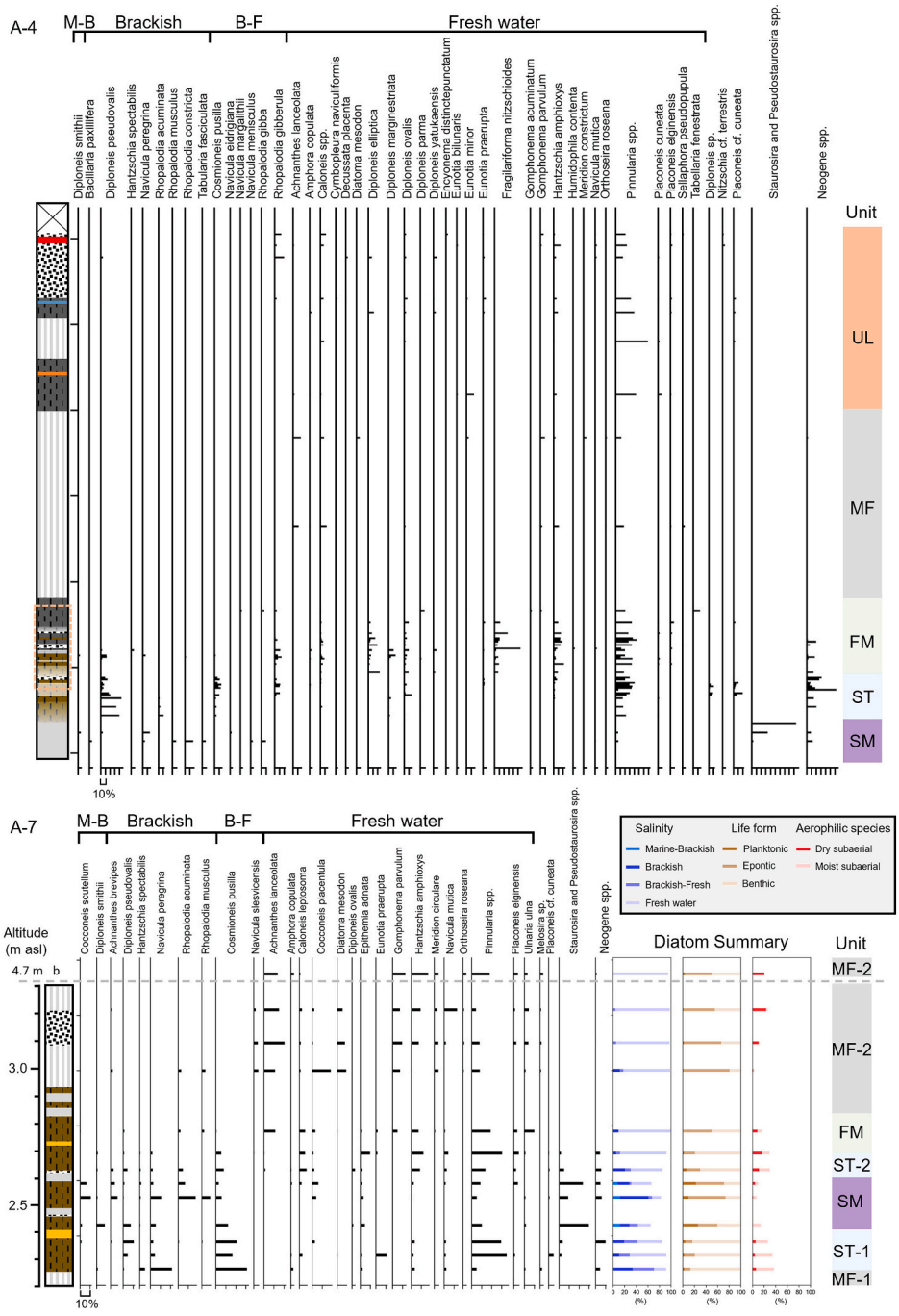

Fig. 4. Summary of diatom analyses for Sites A-4 and A-7. The relative abundance of diatoms is expressed as a percent of the total count. M–B and B–F indicate marine to brackish water species and brackish to freshwater species, respectively. The color bars indicate the sedimentary units, and abbreviations are MF-Mud flow, SM-Saltmarsh, ST-supratidal, FM-Freshwater marsh, and UL-Upland. (For interpretation of the references to color in this figure legend, the reader is referred to the Web version of this article.)

characteristically identified with *Fragilariforma nitzschioides*, which has been reported in streams and side pools (Krammer and Lange-Bertalot, 1991a; Bahls et al., 2018). Unit MF (meaning 'Mud-debris flow') consists of the inorganic white clay, including the freshwater diatoms *Achnanthes lanceolata* addition to component species of Unit FM. The lower black peat of Unit UL (meaning 'Upland') is dominated by *Pinnularia* spp. and includes aerophilic species, such as *Caloneis* spp. and *H. amphioxys*. The Sand HS above B–Tm is similar to the assemblages of lower black peat, including *Rhopalodia* spp.

The TS concentrations showed an increasing trend starting below 3.2 m asl and became more pronounced below 2.6 m asl. The TOC/TS ratios were 20–30 above 2.9 m asl. The silty layers in Unit ST and Unit SM were less than 10 (Fig. 5).

Site A-7. The sediments of Site A-7 were divided into six units based on the diatom inferred depositional environments (Fig. 4). The bottom grayish-white clay layer as Unit MF-1 contained a few diatom valves. Unit ST-1 as the fibrous peat layer shows similar assemblages to Unit ST of A-4, with *C. pusilla*, *D. pseudovalis*, and *N. peregrina* in declining order of prevalence. In Unit SM, the proportion of *C. pusilla* and *Pinnularia* spp. decreases toward the top, and *Staurosira* and *Pseudostaurosira* spp., *Cocconeis scutellum* (an indicator species of sea algae), and *Diploneis smithii*, which is a muddy tidal flat indicator (Chiba and Sawai, 2014), become dominant. Unit ST-2 shows similar assemblages to Unit ST-1, whereas the brackish species as *C. pusilla*, *D. pseudovalis*, and *N. peregrina* decreases than Unit ST-1. Unit FM is dominated by *H. amphioxys* and *Pinnularia* spp., and the assemblages are similar to Unit FM of A-4. The assemblages of Unit MF-2 as the peat unit above Ko-f tephra change to *Meridion circulare*, *A. lanceolata*, and *Gomphonema* spp. The sample at 4.7 m asl showed similar assemblages to Unit MF-2, although the number of diatom valves was few.

Site B-4. At the more inland Site B-4 (Fig. 3), we focused on the boundary between the fibrous peat layer and the lower mud layer to examine environmental changes (Fig. S1). The lower blue-gray clay layer included blackish species such as *N. peregrina* and more than 20% blackish-fresh species. The fibrous peat layer was dominated by the *Aulacoseira* spp. as planktonic freshwater species. Based on ^{14}C dating at the lowermost fibrous peat (Table 1), the date of the change to the fibrous peat layer preceded 1.2 kyr cal BP.

5.3. Mineral composition

Mineral composition analysis was performed by XRD to identify the source of the inorganic sand and mud layers in the ordinary layers (Fig. 6). The thick white clay layer, which included hard shale gravels (Unit MF-2 a-c) in Site A-7, consists of quartz, plagioclase, muscovite, montmorillonite, chlorite, and zeolite. The white clay layer in Site A-4 and the bottom white clay layer (Unit MF-1) in Site A-7 have a similar composition to Unit MF-2a-c. The local present-day beach sand is depleted of zeolite and montmorillonite but rich in K-feldspar, amphibole, and pyroxene. Sand HS in A-4 has the same composition as local present beach sand, henceforth beach sand for short. Sand HC and the overlying mud layer are intermediate in composition between beach sand and Unit MF, including amphibole and zeolite. For the gray clay layer in Site B-2, similar compositions to Sand HC and the overlying mud

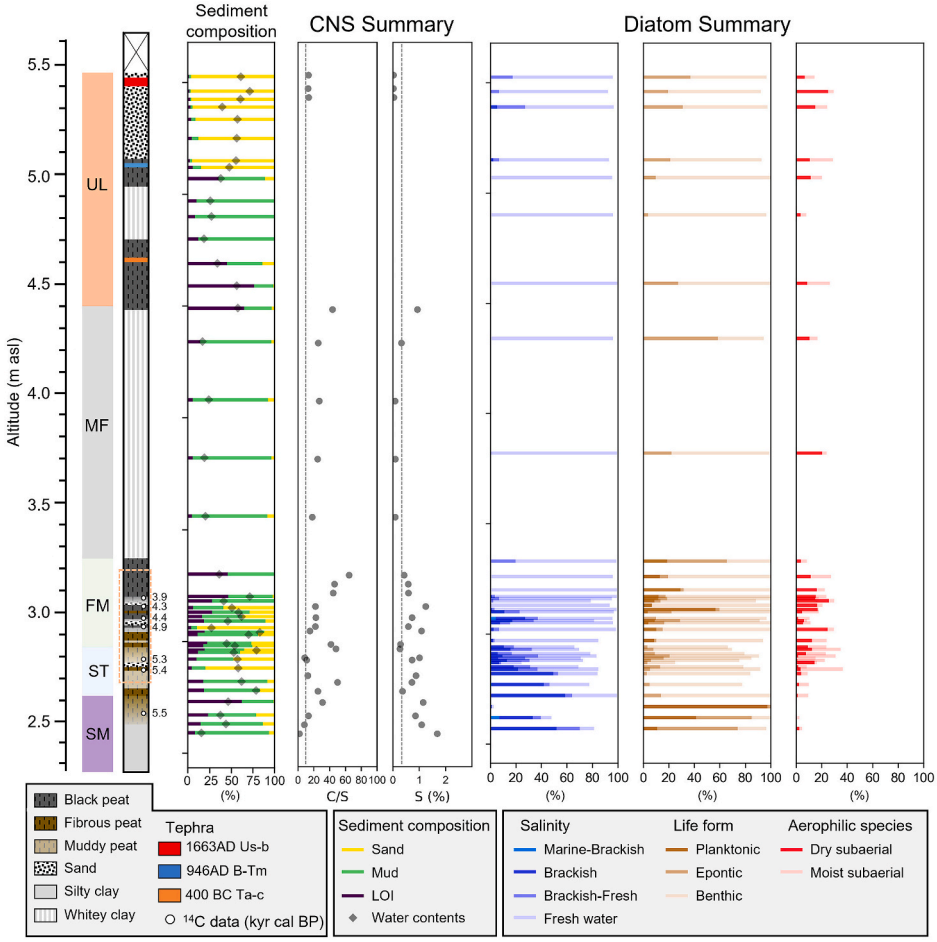

Fig. 5. Site A-4 geochemistry (TOC/TS ratios and TS contents) and sand, mud, organic content (LOI), and diatom assemblage summary (salinity, life form, and the percent of valves of dryness-tolerant species as aerophilic diatom ratio). The color bars indicate the sedimentary units, and the abbreviations are the same as in Fig. 4. (For interpretation of the references to color in this figure legend, the reader is referred to the Web version of this article.)

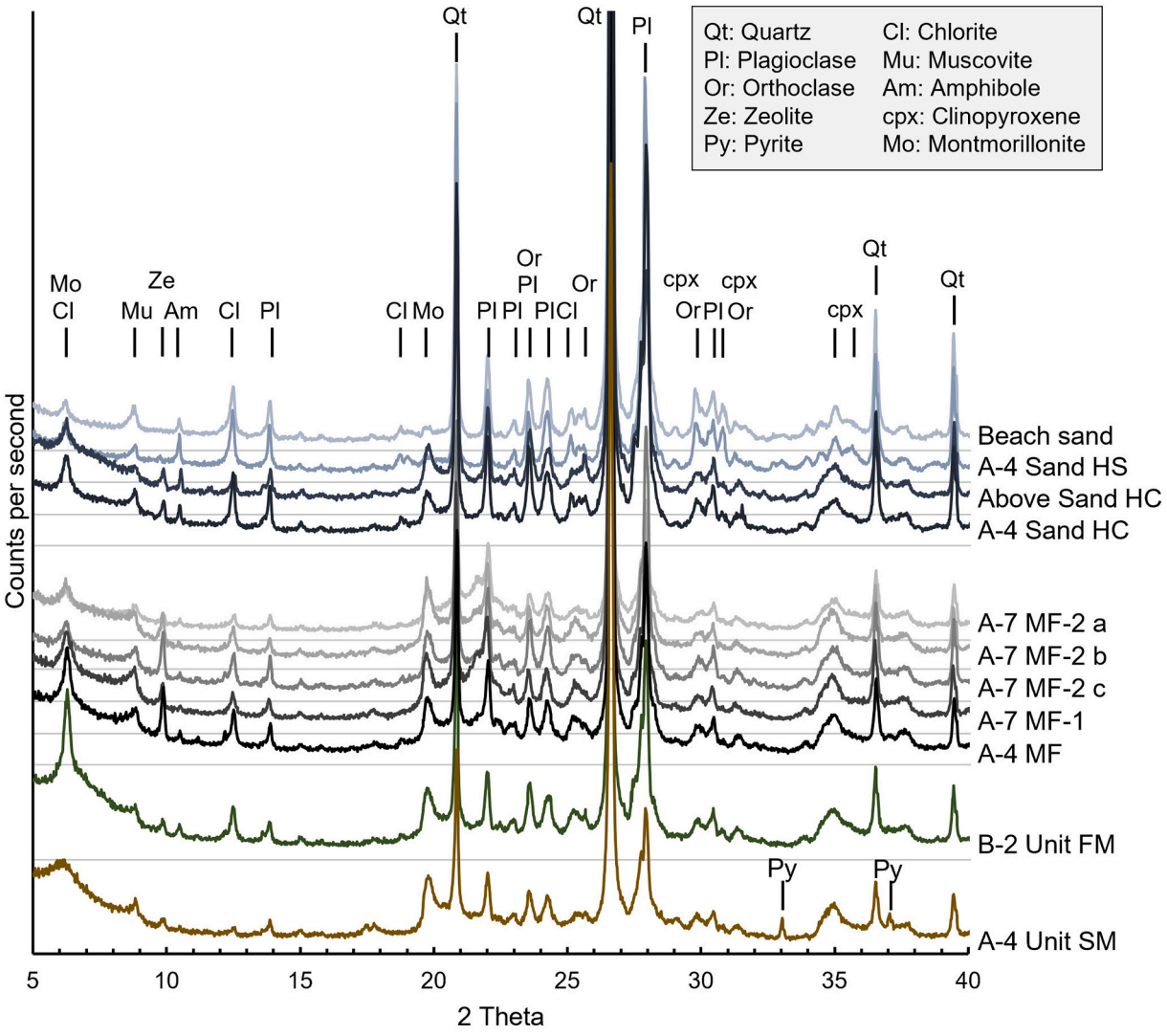

Fig. 6. The results of mineralogy analysis using XRD for the event layers, beach, and ordinary mud layers. The alphabetical symbols are the elements and other minerals for which a 2 theta peak appears.

layer are observed with clay minerals in abundance. The bottom silty clay in Site A-4 contains pyrite in addition to a composition otherwise similar to MF-2 sample.

5.4. Features of the sand layers

Sand HS was deposited after the 10th century, located from tephra B–Tm to above Us-b. Based on radiocarbon dating, Sand HA, HB, and HC were deposited in 4.3–3.9, 4.9–4.4, and 5.4–5.3 kyr cal BP, respectively (Table 1). Sand HS is widely distributed in outcrops along the coast with a thickness of several tens of centimeters. Sand HS had unclear boundaries with the peat layer and a homogenous structure. Sand HA is ~1 cm thick and overlain by a grayish-white silty clay layer (mHA: Figs. 3b and 7). The grain size compositions of Sand HA indicate a mode at ~1.2 phi with a fine-grained tail (Fig. 8). Sand HB are of 1–3 cm thickness, overlaid by the grayish-white silty clay layer (mHB), and the grain size compositions are well-sorted with a mode of ~1.1 phi. Sand HC is of 1–9 cm thickness and has a slight degree of normal grading: it will eventually become silty (mHC). The grain size compositions have a mode at ~1.7 phi and a tail to the fine-grained component. In the western cores, the sand layers were found to be sometimes interbedded with mud layers and tended to be thicker (Fig. 3b). Sands HA, HB, and HC were not observed in Site A-7 or Line B.

The diatom valves in Sands HA, HB, and HC are dominated by Neogene diatoms in addition to species below the sand layers (Fig. 9). The proportion of Neogene diatom valves tends to decrease upward from the sand layers, which is significant in Sand HC. The mud layers above the sand layers contain slightly more brackish species than below the sand layers, and the proportion decreases upward, whereas *H. amphioxys* tends to increase. Sand HS shows similar assemblages to below peat layer and does not contain Neogene fossils.

The chemical composition and physical properties were obtained for the profile from Sand HA to Sand HC (Fig. 7). The CT values peaked at the sand layers and gradually decreased up to 5 cm above the sand layers. The chemical composition profiles of Si, K, and Ti show the same trend as the CT values. The Ca and Sr peaked only in the stratigraphic levels where the CT values exceeded 1000. The XRD results suggest that these elemental peaks are caused by K-feldspar and amphibole. The Mo ratios inversely correlate with CT values. For the CT values and chemical composition profiles, the mud layers above Sand HA and HB show a general decreasing trend, whereas that of Sand HC displays several fluctuations.

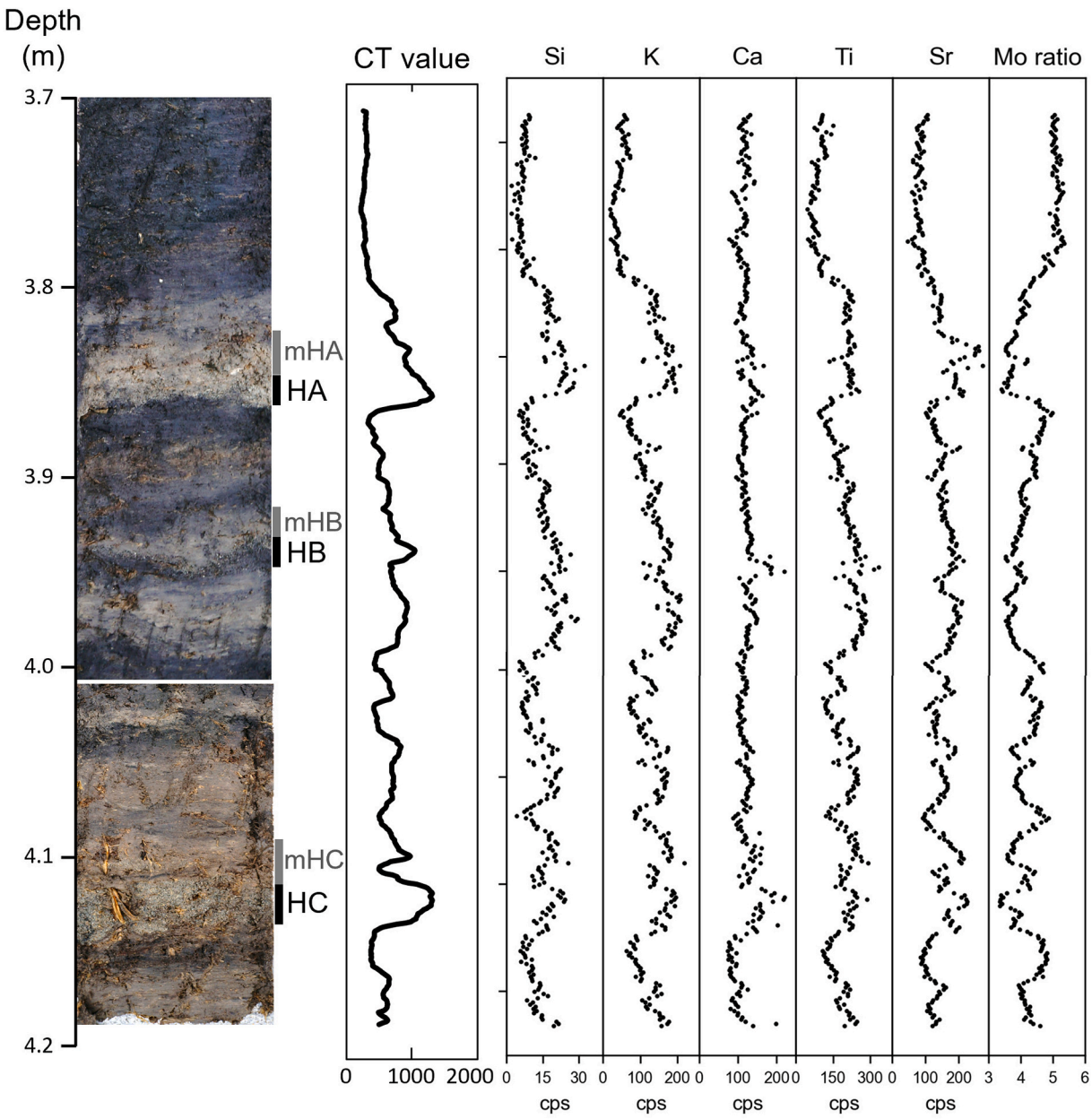

Fig. 7. CT values and chemical composition profile changes by X-ray CT and XRF scanner for the Site A-4 core.

6. Discussion

6.1. Reconstruction of paleo-sea-level and depositional environment

The RSL changes and associated changes in depositional environments were reconstructed based on diatom assemblages and chemical analyses (Fig. 10). Unit MF-1 of Site A-7 contained few diatom valves, and no traces of marine sediments such as pyrite were observed (Fig. 6). This unit was interpreted to be debris flow deposits because of the presence of Neogene hard shale gravels including zeolite, as discussed further below concerning Unit DF-2. Many slope failure topographies have been reported along the Hidaka coast (Yanai and Igarashi, 1990), and Unit MF-1 is interpreted as one of these event sediments.

Unit ST-1 in A-7 is presumed to be a supratidal environment because of the salt-tolerant blackish-fresh water species as *C. pusilla* and *D. pseudovalis*, which are reported to emerge at HAT (Sato et al., 1983; Sato, 2002; Zong and Sawai, 2015), and the increasing proportion of brackish water species suggests that the sea-level rise continued until 6.5 kyr cal BP (Fig. 4).

Unit SM is considered to have been the saltmarsh (or endgame of a tidal flat environment) because of brackish water species accounting for more than 30%, such as *T. fasciculata*, *C. scutellum*, *D. smithii*, and *N. peregrina*. *T. fasciculata*, *C. scutellum* are reported indicator species of seawater algal beds, and *D. smithii* is a muddy tidal flat indicator (Chiba and Sawai, 2014). *N. peregrina* has been reported to emerge widely in highmarsh to lowmarsh along the coast of Hokkaido (Sawai et al., 2004a). The presence of pyrite (Fig. 6), which is produced by sulfate-reducing bacteria in seawater, and the high TS content relative to TOC, support this interpretation (Fig. 5). The distribution of these saltmarshes extended at least up to B-4 along Line B as the blue-gray mud layers, suggesting that there was a tidal flow running up until ~2000 BP (Fig. 10). The timing of peat formation was earlier at sites farther from the Fuji River, such as Site D. Thereafter, the unit became dominated by *Staurosira*, *Pseudostaurosira*, and *Aulacoseira* spp., which suggests that the inland area became a closed freshwater area, and the seaward area became a closed brackish water area after the cessation of sea-level rise (Fig. 4).

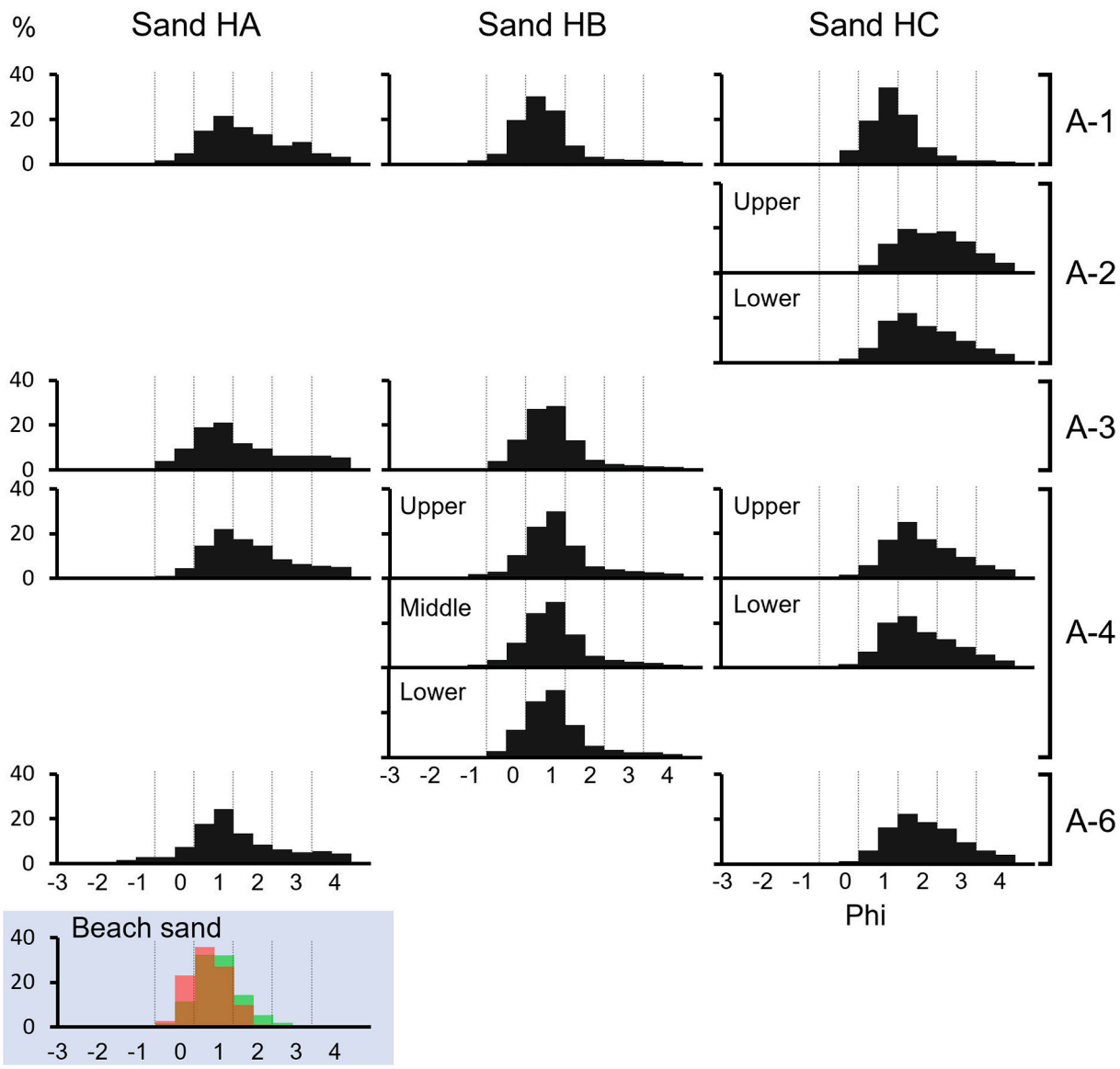

Fig. 8. Grain size histogram of the event sand layers and beach sand.

Unit ST-2 is dominated by *D. pseudovalis* and *C. pusilla*, which are found at the end of the HHS period (Sato et al., 1983; Sato, 2002; Zong and Sawai, 2015), species that account for 30%–40% of the total; therefore, salinity is estimated to have decreased as the area became supratidal during this period.

Unit FM have emerged from the seawater since the time in which the assemblages changed to benthic freshwater species, such as *Pinnularia* spp., including planktonic species. (Fig. 4). This unit is presumed to be a frequent water stagnant environment, as it includes species that inhabit a stream or pool such as *F. nitzschioides*, while it includes some dry-tolerant species. The emergence ages in Site A-4 are earlier than that in Site A-7 because the change from Unit ST to FM is estimated to be 5.0 kyr cal BP and 6.3 kyr cal BP for Site A-4 and Site A-7, respectively. Therefore, Site A-7 was considered to be farther from the coastline (Fig. 10). The aerial photograph shows a basement below the sea surface near Site A-7 (Fig. 2b), which is inferred to be the anticlinal part of the fold structure. The beach ridges and interdunal wetlands were assumed to form along the anticlines considering that river meanders are influenced by the fold structures (Fig. 2). It is presumed that seawater entered from the area around the present river mouth, which is consistent with the discrepancy in the emergence age of both sites. The gray clay layers above the blue-gray clay in Line B are correlated with Unit FM because the diatom assemblage indicates a freshwater marsh environment (Fig. S1), but this layer also transitions to floodplain deposits, since the gray clay layer in Site B-2 consists of mineral compositions of intermediate between Neogene bedrock and beach sand (Fig. 6).

Unit MF-2 is locally thick in A-7 and is an inorganic clay layer containing Neogene hard shale, which is difficult to interpret as a layer that is gradually deposited over a long period of time. The distribution of a terrace consisting of Neogene hard shale behind Line A suggests that this unit was formed by slope failure and associated mud-debris flows (Yanai and Igarashi, 1990). The presence of zeolites indicates a detrital supply from Miocene marine sedimentary rocks since zeolites are known to be commonly derived from the very slow alteration of volcanic glasses in seawater (Hay and Sheppard, 2001). Unit MF in Site A-4 shows a similar mineral composition and diatom assemblages to Unit MF-2 in Site A-7. The mud layers in Site A-4 are chronologically comparable with the mud layers in Site A-7 (Figs. 3 and 4), suggesting that the mud-debris flow deposits were derived from a slope failure that occurred at 4000–3000 BP (Fig. 10). This is supported by the fact that a fan-shaped topography is observed in the gully behind Sites A-4 and A-7 (Fig. 2b). Yanai and Igarashi (1990) reported that pollen analysis in the northern Hidaka

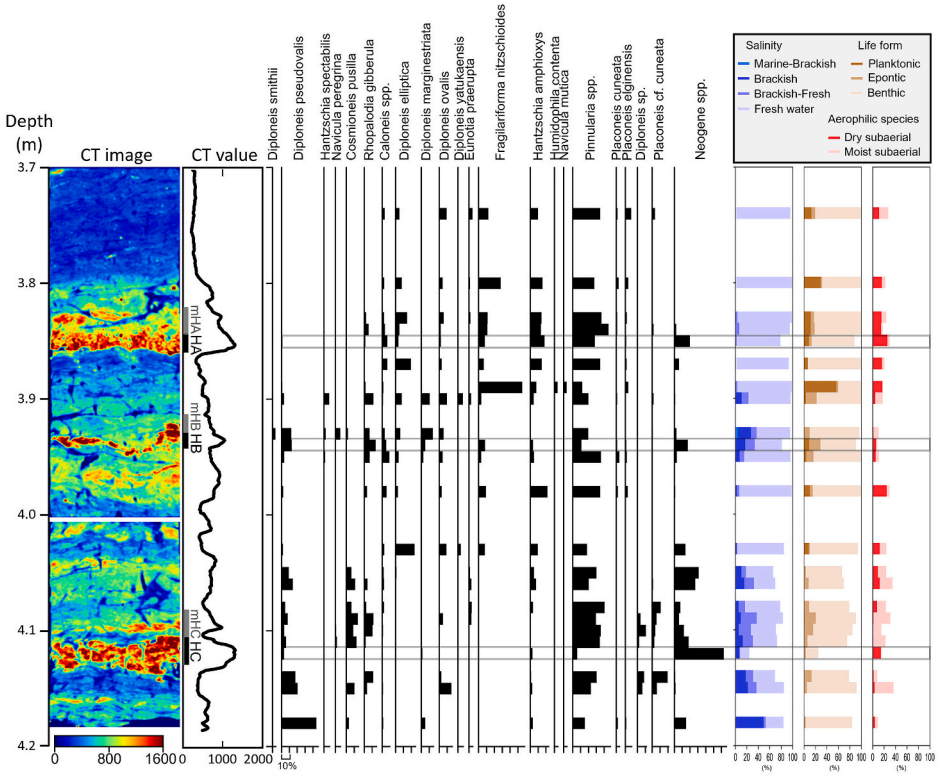

Fig. 9. CT image and detailed diatom assemblage summary around the event layers.

region revealed a transition from a warm to a cool humid climate at ~2600 BP and that this climatic change stimulated freezing and thawing activities, resulting in more frequent slope failures. The mud layers are assumed to have been formed by multiple mud-debris flows because they are interbedded with peat layers (Fig. 3).

For Unit UL, the basement was raised by slope failure sediments (Unit MF), resulting in a more terrestrial environment in the form of a dominating upland, which was filled with aerophilous or benthic freshwater species (Fig. 4). On the other hand, Site C near the river mouth was a high-energy environment even around the 17th century, with sand and silt predominating (Fig. 3). The predominance of sand sediments in Unit UL since the 10th century suggests that the present shoreline position was changed by coastal erosion.

The RSL change in this area is estimated from SLIPs obtained by this study considering the change in the depositional environment (Table 2, Fig. 11). The RSL change curves around the Shimokita Peninsula, where the influence of crustal deformation is small, are estimated from the GIA model and SLIPs (Yokoyama et al., 2012). The SLIPs are reported in the Shizunai and Utoma areas along the Hidaka coast. In Utoma, sea regression began around 3.5 kyr cal BP and the altitude of the local HHS is reported to be 2–3 m asl (Nakanishi et al., 2020a). In the Shizunai area, the HHS period continued until ~4.0 kyr cal BP, when the sea level at that time was 4–5 m asl before falling to 1.0–1.5 m asl at 1.5–1.0 kyr cal BP (Nakanishi et al., 2022a). The elevations and ages of the newly obtained SLIPs as supratidal and high marsh in this area are shown in Fig. 11. These SLIPs are 1.5–2.5 m higher than the curve based on the GIA model for the Shimokita Peninsula. The long-term crustal deformation trend in this region is estimated to be 0.3–0.5 mm/year based on the elevation of the MIS 5e and MIS 7 marine terraces. The RSL changes shown by SLIPs in Harutachi are consistent with the RSL curve reflecting an uplift rate of ~0.3 mm/year. The SLIPs of Utoma are in good agreement with the RSL curve in the Harutachi area. On the other hand, the SLIPs of the Shizunai area, at the adjacent Harutachi area, are 1–3 m higher than the curve estimated from the uplift rate of 0.3–0.5 mm/year. The reason for this difference in paleo-sea levels in the adjacent areas may be related to the location of the fold structures. Shizunai is in an uplifted area adjacent to the Harutachi anticline, and Harutachi is located near a minor syncline between the Otoe syncline and the Harutachi anticline (Fig. 2). Because Shizunai is distributed in the uplift zone of the folding movement and Harutachi is distributed in the subsidence area, it is inferred that there was a difference in local uplift trends between the two areas. This structural movement has probably occurred, in either a continuous or a punctuated change, for the past several thousand years.

6.2. *Formation factors of the sand layers*

We sought to determine whether the sand layers were event layers caused by extreme waves, based on the sedimentological features and the depositional environment. Sand HS has an unclear boundary with peat, a homogeneous sedimentary structure. While modern tsunami deposits have sedimentary structures that reflect abrupt and strong flows such as clear contacts and single or multiple grading structures (Morton et al., 2007; Takashimizu et al., 2012), Sand HS, which shows continuous deposition across the Us-b tephra, has no positive evidence as an event layer. The sand source was the adjacent beach, as it exhibits a mineral composition very similar to that of the present beach sand (Fig. 6). The diatom assemblage indicated a freshwater marsh or an upland environment, and allochthonous diatoms were not detected (Fig. 4). The 1948 aerial photograph also shows the site of our Line A to be covered with sand due to significant beach erosion (Fig. 2), and the beach sand has likely been transported to the upland as aeolian sand. However, since tsunami deposits derived from the Kuril Trench earthquake have been reported between Us-b and B–Tm in the Shizunai area (Nakanishi et al., 2022a), the possibility that Sand HS contains tsunami deposits cannot be excluded.

Sands HA, HB, and HC show a clear basal contact and are distributed as continuous thin layers in the horizontal direction (Fig. 3b). The grain size and mineral compositions of these sands are similar to beach sand (Figs. 6 and 8), and the absence of other sandy sediments in the

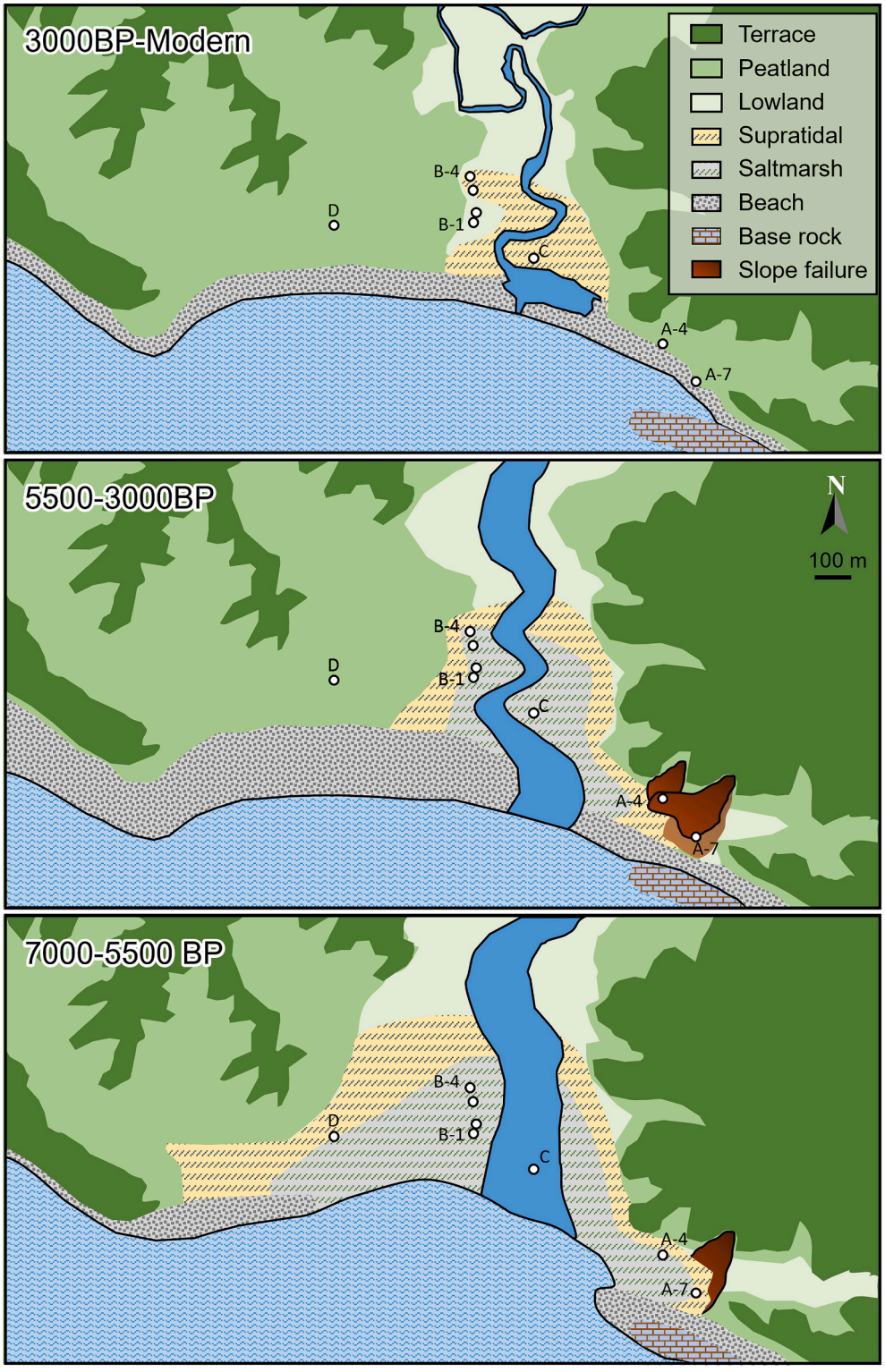

Fig. 10. Sketches of the reconstructed evolution of the depositional environment in the Harutachi area over the past 7000 years.

surrounding area indicates that beach sand is a reasonable source of sand. The grain size tends to become finer toward the east, which is estimated to be the inland side at 5.5–4.0 kyr cal BP (Figs, 8 and 10). These sand layers contain diatom species living in environments interpreted as being more seaward than the mud layers below the sand layers, which also contain a high proportion of Neogene species (Fig. 9). The high proportion of Neogene species and zeolite in these sand layers is interpreted to rework sediments from the Neogene sedimentary rocks, suggesting that they originate from the erosion and transport of sand and mud from the seaside and backshore terrace due to extreme waves.

The mud layers (mHA, mHB, and mHC) above the sand layers show a continuous decrease in CT values indicating submerged densities and elemental profiles (Si, K, Ti, and Sr) upward (Fig. 7), which can be interpreted as a sequential environmental change continuing from months to years or a single normal grading structure. The former scenario is known to be associated with both sudden subsidence and

Table 2
Summary of the sea level index point dataset in the Harutachi area.

Site	Elevation	Material	2θ age (cal. yr BP)		Depositional environment	Indicative tidal	Reference	Evidence
	(m asl)	dated	mean	age error	boundary	upper limit	water level	
A-4	2.8	Plant fragment	5294	±156	Supratidal/ Freshwater marsh	HAT	MSL + 0.6 m	*Cosmioneis pusilla*, and *Diploneis pseudovalis*. TOC/TS 10–20. TS 0.3%–1%
A-4	2.6	Wood fragment	5459	±127	Highmarsh/ Supratidal	MHHW	MSL +0.4 m	*Navicula peregrina, Tabularia fasciculata, Staurosira* and *Pseudostaurosira* spp. TOC/TS < 10. TS > 1%. Pyrite.
A-7	2.7	Wood fragment	6299	±110	Supratidal/ Freshwater marsh	HAT	MSL +0.6 m	*C. pusilla, D. pseudovalis*, and *N. peregrina*
A-7	2.6	Tephra Ko-f	6303	±91	Highmarsh/ Supratidal	MHHW	MSL +0.4 m	*T. fasciculata, C. scutellum, Diploneis smithii, N. peregrina, Staurosira and Pseudostaurosira* spp.
A-7	2.4	Tephra Ko-g	6550	±50	Supratidal/ Highmarsh	HAT	MSL +0.4 m	*C. pusilla, D. pseudovalis*, and *N. peregrina*

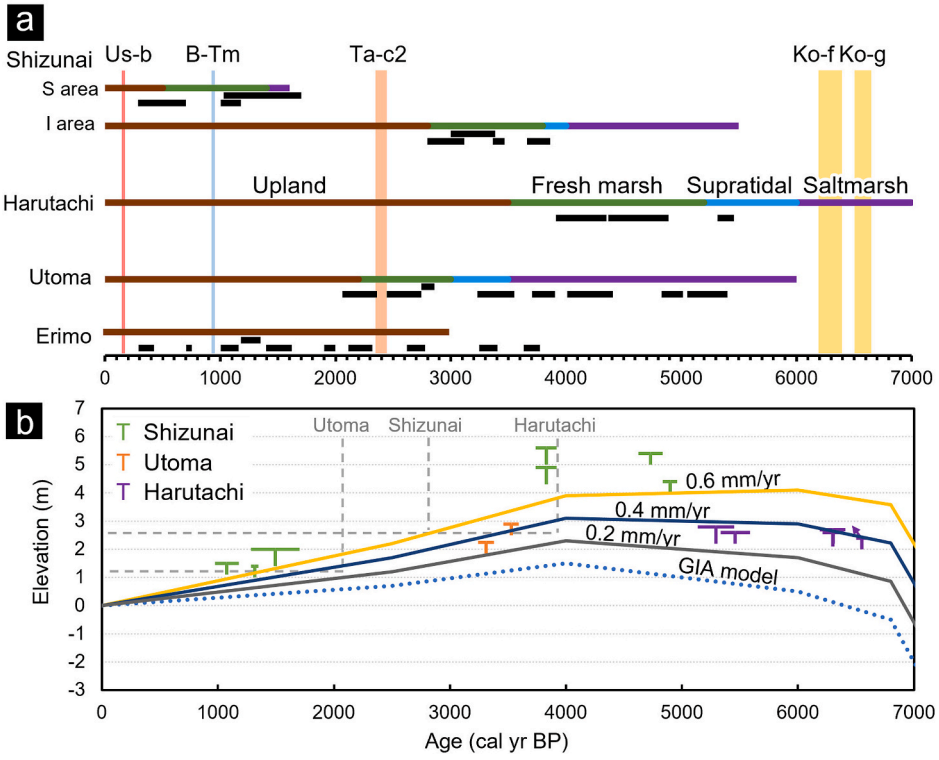

Fig. 11. The depositional environments in which the event layers were preserved and reconstructed sea-level changes that caused depositional environmental changes in the Hidaka coastal region. The data for the Shizunai area are referenced from Nakanishi et al. (2022a), those for the Utoma area are referenced from Nakanishi et al. (2020a), and those for the Erimo area are referenced from Nakanishi et al. (2022b). (a) Depositional ages of event layers and evolution of depositional environments reported along the Hidaka coast during the past 7000 years. Black bars represent the dating results (2σ) of the event layers. The color bars show the period of each depositional environment. The vertical color columns indicate the age and distribution of the widespread tephras. (b) The estimated SLIPs and RSL change curves in the Hidaka coastal region. The T-shape symbols display the altitude and ^{14}C age of the SLIPs as the upper limits of MHHW or HAT based on the geological evidence. The width and height of the T-shape symbols indicate the error from dating and the difference in altitude from MSL, respectively. The blue dotted line is the Holocene sea-level prediction based on the GIA model in the Shimokita Peninsula (Yokoyama et al., 2012). The solid lines show the RSL change curve calibrated by uplift rates on the range based on the MIS 5e and 7 marine terrace heights along the Hidaka coats (0.2, 0.4, and 0.6 mm/year). The gray dashed lines indicate when the event layers were first identified in each area and the RSL for that time period as estimated from the RSL curves. (For interpretation of the references to color in this figure legend, the reader is referred to the Web version of this article.)

gradual uplift movements (Atwater et al., 2004; Sawai et al., 2004b). The mHB layer may have been generated by subsidence movement because of the temporary increase in brackish species (Fig. 9). The mHB and mHC layers have an increasing number of dry subaerial species, such as *H. amphioxys* upward, suggesting that it was gradually drained (or uplifted) and changed to a drier environment after the event. Otherwise, the formation of a temporary mud inflow environment for a relatively short period associated with beach scouring is also a possibility (Fujiwara et al., 2013; Sawai et al., 2015). The latter scenario is one in which the mud layers above the sand layers were derived from a sequence of mud drapes (also known as forming mud caps) carried by tsunamis (Richmond et al., 2012; Takashimizu et al., 2012). The continuous change in CT values and the not much change in the diatom assemblages may support the scenario that the mud layers above the sand layers are mud caps (Fig. 9). In any case, the sedimentological features of the sand layers and their mud overlays are thus consistent with tsunamis and earthquakes.

The depositional ages of these sand layers were compared with those of tsunami deposits reported along the Pacific coast of Hokkaido (Fig. 11). The three sand layers can be compared with the U6, U7, and U8 layers in Utoma (Nakanishi et al., 2020a), which were slightly closer to the Kuril Trench, suggesting that Sands HA, HB, and HC in Harutachi are the tsunami deposits that reached the Hidaka region.

Extreme waves from the sea are storm surges as a possible source in addition to tsunamis. The typhoons in the Hidaka region in the last 70 years are summarized in Nakanishi and Ashi (2022), and the maximum wind speed was 80 kt and the minimum pressure was 965 hPa due to the Hidaka region is far from the tropical zone. The results of sediment transport modeling by the largest typhoon model in Hokkaido in the adjacent Shizunai area showed that the sediment distribution was

limited to a river mouth or beach zone (Nakanishi and Ashi, 2022). The depositional age intervals of several hundred years likely also distinguish them from the highly frequent deposition derived from storms. However, it is difficult to determine if tsunamis were the only type of inundation that might have formed these sand layers because the sand layer distribution (shoreline location and the extent of sand layers further inland) is unclear due to the difficulty of further investigation. The depositional period of the event layers in this area will add to what we already know about earthquake and tsunami periodicity from the archives of the Shizunai area (Nakanishi et al., 2022a). It is suggested that additional work is required to clarify the origin of the event layers in Harutachi as it will be most valuable as a guide for future civil defense.

6.3. Preservation and formation of event layers

To clarify the relationship between the formation and preservation periods of the event layers and the depositional environment, the age of the event layers and the depositional environment changes caused by RSL changes along the Hidaka coast are jointly summarized (Fig. 11). The depositional period of the event layers in the Harutachi area was the period during which supratidal to freshwater marsh environments were distributed at Site A-4. The sand layers were not identified as having been deposited in the saltmarsh or upland environments.

Saltmarsh environments are estimated to have low preservation potential because the disturbance rate exceeds the sedimentation rate (Wheatcroft, 1990; Leorri et al., 2009; Spiske et al., 2013). A thin event layer will normally be eroded in the face of such powerful forces and be disturbed by bioturbation in a tidal zone. Also, a tsunami inundation including sand may be discharged by outflow to the sea due to the underdeveloped nature of the beach ridge (Nakanishi and Ashi, 2022). In the upland environment, the formation of a beach ridge and the regression of the shoreline are liable to prevent the extreme waves from transporting sand to the site away from the shoreline. Also, the preservation potential of event layers may be lower in an upland environment because of the lower sedimentation rate and long duration of weathering as compared to a wetland environment (Wheatcroft, 1990). Therefore, a thin sand layer may not be preserved even if waves reach the site; in this study, no evidence of inundation was found in Unit UL due to the low sand content (Fig. 5). Well-preserved event layers are most likely to be found between these two extremes of an overly seaward and an overly landward environment. In other words, the conditions under which the event layer is likely to form depend on depositional environments and the distance from the shoreline.

The depositional environment in which sand layers were preserved in the Harutachi area is very similar to that of the adjacent Shizunai area. The diatom assemblages indicate that the depositional environment during this period was after the establishment of a closed environment from brackish water, dominated by small *Fragilaria* spp. such as *Staurosira* and *Pseudostaurosira* spp. (Fig. 4: Stabell, 1985; Ludikova et al., 2020; Nakanishi et al., 2022a), indicating that the long period of isolation from seawater enhanced the preservation of the event layers. The upper limit of the event layer is a closed environment with water depth, which prevented the discharge of sand and mud and post-depositional erosion. The deposition in such environments is supported by the presence of mud caps indicating long water stagnation and the distinct normal grading structures (Fig. 7). Therefore, freshwater marsh and supratidal environments are suitable depositional environments for the preservation of event layers.

The tsunami wave heights must have been similar between Shizunai and Harutachi; on the other hand, the depositional ages of the event layers in both areas do not overlap (4.0–3.0 and 5.5–4.0 kyr cal BP). The difference is due to the relationship between the location of the survey sites and shoreline locations, which reflects the coastal evolution process unique to each coast. The Utoma area has preserved event layers in more diverse environments, over the HHS and the subsequent regression of the sea from the saltmarshes to the early upland environment (5.5–2.0 kyr cal BP: Nakanishi et al., 2020a). The tsunami deposits were presumably preserved in the saltmarshes because the thickness of the event layers exceeded the depth of disturbance (Wheatcroft, 1990). The thickness of the sand layer in this area has been reported to be thicker at the higher estimated RSL (Nakanishi et al., 2020a), and it could be preserved from disturbance even in a saltmarsh environment. The Erimo area, which faces the Kuril Trench, has been an upland environment since at least 2.4 kyr cal BP (Nakanishi et al., 2022b), and the event layers are preserved even the upland environment (Fig. 11). This suggests that in areas where high tsunami wave heights are observed, tsunami inundation reached even the upland environment away from the coastline, leaving thick sand layers that could withstand weathering. The formation of the event layers in the area facing trenches is not very sensitive to the depositional environment.

When comparing areas along the Hidaka coast, the event layers were distributed only in the limited depositional environment at the distant areas from the Kuril Trench (Fig. 11). Successive tsunamis generated by Kuril Trench earthquakes are plausible candidates for the origin of these event layers because many of the event layers from Utoma to Shizunai are correlated with the tsunami events in eastern Hokkaido based on chronology and numerical simulations (Nakanishi and Ashi, 2022; Nakanishi et al., 2022a). Since the wave heights tend to decrease toward the northwest of the Hidaka coast in the 17th-century tsunami simulation (Nakanishi et al., 2022b), smaller wave heights are expected in the Shizunai and Harutachi areas compared to the Utoma area. In other words, the greater the distance from the trench, the less tsunami inundation will reach the inland environment (i.e., upland).

Fig. 12 shows the formalization of the conditions under which an event layer is preserved depending on the distance from the trench and the distance from the coastline or differences in the depositional environment. It is assumed here that the depositional environment changes from saltmarsh to upland environments with distance from the shoreline; actually, it varies depending on the topography, coastal evolution pattern, and climate condition. The different depths of core samples obtained at a given point seem to move in position relative to the shoreline due to shoreline migration associated with RSL changes (e.g., the shallow depth indicates a more inland environment during a period of sea-level fall).

First, high wave heights and inundation extents are unquestionably the dominant factor in sand layer formation in that an extreme inundation transports sand to broad coastal environments even an upland. In general, deeper inundation depths form thicker sand layers, which also have an advantage for post-depositional preservation on even saltmarshes and tidal flats. Second, the shoreline migration associated with the RSL rise will result in relatively more inland inundation. On the other hand, it also makes saltmarshes and tidal flats wider, thus reducing post-depositional preservation in zones closer to the shoreline. Third, a thin event layer is more sensitive to local depositional environments. If only a thin sand layer is formed near saltmarshes in a region away from the trench due to small wave heights, the disturbance depth will exceed the sand thickness and the sand layer will not be preserved (Wheatcroft, 1990). Even if inundation transports sand to an environment farther inland than the saltmarsh, the thin sand layer often will not be preserved if there was a steady flow or if it is exposed on dry land with weathering.

Therefore, event layers in distant areas from wave sources would be observed to be concentrated only in certain stratigraphic levels. An area of the coastal zone where an event layer is preserved is limited to wetland environments at the time of the event; thus, which period is archived depends on the survey point (i.e., distance from the shoreline and depositional environment). Coastal erosion (e.g., Harutachi and Utoma) and the narrow beach-ridge plain (e.g., Shizunai) make comprehensive surveys difficult, resulting in a fragmented and short time window for event archives in distant areas. However, understanding the specific depositional environment suitable for preservation can advance the investigation and the event history reconstruction using tsunami deposits to an advantage.

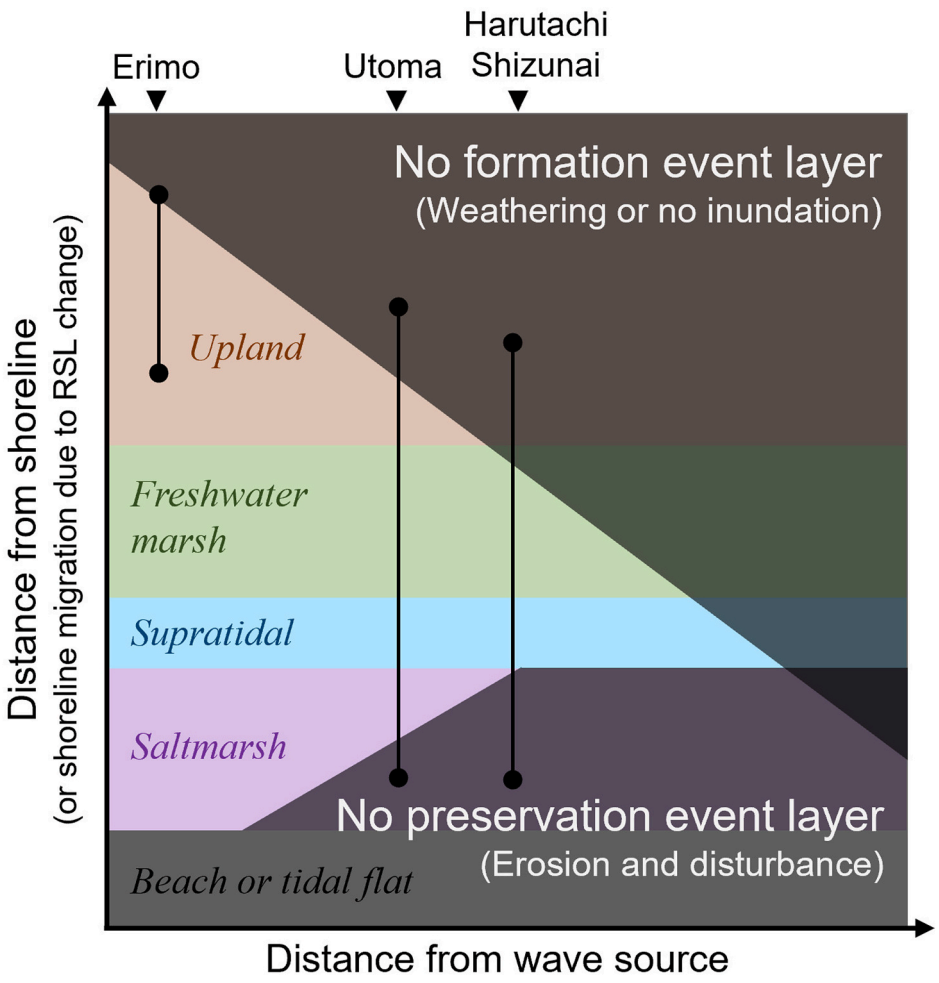

Fig. 12. Schematic diagram showing the preservability of the event archive dependent on the distance from the wave source and the distance from the shoreline. It is assumed that the depositional environment varies with distance from the shoreline. Black shadows indicate zones of low preservability of event layers. The solid black lines indicate the extent of the study targets in each area, which includes the horizontal extent of the study area from the shoreline and the relative change in depositional environment due to sea transgression-regression corresponding to the core depths.

6.4. Tsunami damage impacts from future sea level rise on the Hidaka coast

On the Hidaka coast, it seems unlikely that even a tsunami from an M > 8 Kuril Trench earthquake at present sea level would form a sand layer beyond the barrier. According to the geological records in the Utoma to Shizunai areas, the event layers were formed when the sea level was ~1.2 m higher than present in the southern Hidaka region (Utoma: when the uplift rate is 0.3 mm/yr) and when the sea level was ~2.7 m or higher in the central Hidaka region (Shizunai and Harutachi: when the uplift rate is 0.6 and 0.3 mm/yr, respectively), respectively (Fig. 11). Although an exact comparison cannot be made because of the global sea level rise projections, it is estimated that if current greenhouse gas emissions continue, sea level will rise by 1 m in AD 2100 from AD 1900 (Arias et al., 2021; Dura et al., 2021). The low-likelihood scenarios including ice-sheet instability processes could result in a 2-m rise in sea level. It is possible that a tsunami strikes the Hidaka coast as large enough to transport sediments in a back-barrier area within 100 years from now (whether or not a tsunami would occur is another matter).

However, the strong influence of coastal topography and depositional environment suggests that there may not be a simple positive correlation between sea-level height and event layer distribution. Future risk assessments of extreme wave events should more strongly recognize the possibility that not only sea-level rise but also accompanying changes in coastal topography may contribute to the severity of disasters, especially in regions far from tsunami sources.

7. Conclusion

This study investigated the depositional environments and the event layers over the past 7000 years in Harutachi on the Hidaka coast. Based on diatom assemblages and chemical analysis, mid-Holocene highstand was identified between 7.0 and 5.0 kyr cal BP, which was accompanied by the development of saltmarshes and their transition to freshwater marshes. Three thin layers of horizontally continuous sand were identified, with clear boundaries and similar grain size and mineral composition to beach sand. The inorganic mud layers overlying the sand layers exhibited similar chemical and mineral composition to the sand layers and contained brackish and Neogene diatom species, suggesting that these must be derived from mud drapes. The fact that these event layers can be chronologically correlated with the tsunami deposits in Utoma also suggests that they may be tsunami-related deposits.

The formation of the event layers was limited to supratidal to freshwater marsh environments associated with regression. This association has also been observed in adjacent areas, which suggests that these supratidal to freshwater marsh environments are the most favorable for the formation and preservation of event layers. In areas closer to the Kuril Trench, the depositional environments for the preservation of event layers tended to become more diverse. Because the tsunamis are larger than distant areas, their deposits in an area facing trenches are typically transported further inland even in an upland environment, and take longer to erode even in a saltmarsh environment because of more massive sand.

In sum, the depositional environment in which the event layers were well preserved can be explained uniformly along the entire Hidaka

coast. The preservability of event archives basically depends on the degree to which the wave is attenuated in its travel from the wave source. Second, changes in shoreline position and depositional environment as a result of sea-level change contribute to the distribution and preservation of an event layer. Moreover, the archive preservability in distant areas is influenced by the in-situ specific depositional environments such as a water or closed environment. The features of the depositional environment related to preservation are likely to be similar in the ice sheet far-field regions in a cool temperate zone that forms peats, which is a suitable condition for research to clarify tsunami history. The identification of a depositional environment in which event layers are likely to be preserved will provide information that will help to improve future investigations of coastal hazards.

Declaration of competing interest

The authors declare that they have no known competing financial interests or personal relationships that could have appeared to influence the work reported in this paper.

Data availability

Data will be made available on request.

Acknowledgments

Field surveys were assisted by Y. Okuma and T. Kochi (Atmosphere and Ocean Research Institute, The University of Tokyo). We thank the three anonymous reviewers for their helpful comments on the paper. This work was supported by JSPS as Grants-in-Aid for JSPS Fellows Grant Number JP20J21239. This study was performed under the cooperative research program of the Center for Advanced Marine Core Research (CMCR), Kochi University <Accept No. 20A010 and 21B042>.

Appendix A. Supplementary data

Supplementary data to this article can be found online at https://doi.org/10.1016/j.qsa.2023.100081.

References

Arias, P.A., Bellouin, N., Jones, R.G., Naik, V., Plattner, G.-K., Rogelj, J., Sillmann, J., Storelvmo, T., Thorne, P.W., Trewin, B., Rao, K.A., Adhikary, B., Allan, R.P., Armour, K., Barimalala, R., Canadell, J.G., Cassou, C., Cherchi, A., Collins, W., Corti, S., Cruz, F., Dentener, F.J., Dereczynski, C., Luca, A.D., Diongue, A., Doblas-Reyes, F.J., Dosio, A., Douville, H., Engelbrecht, F., Fyfe, J.C., Gillett, N.P., Goldfarb, L., 2021. Climate Change 2021: the Physical Science Basis. Contribution of Working Group14 I to the Sixth Assessment Report of the Intergovernmental Panel on Climate Change. Technical Summary.

Atwater, B.F., Furukawa, R., Hemphill-Haley, E., Ikeda, Y., Kashima, K., Kawase, K., Kelsey, H.M., Moore, A.L., Nanayama, F., Nishimura, Y., Odagiri, S., Ota, Y., Park, S.-C., Satake, K., Sawai, Y., Shimokawa, K., 2004. Seventeenth-century uplift in eastern Hokkaido, Japan. Holocene 14, 487–501. https://doi.org/10.1191/0959683604hl726rp.

Bahls, L., Boynton, B., Johnston, B., 2018. Atlas of diatoms (Bacillariophyta) from diverse habitats in remote regions of western Canada. PhytoKeys 1–186. https://doi.org/10.3897/phytokeys.105.23806.

Berner, R.A., Raiswell, R., 1984. C/S method for distinguishing freshwater from marine sedimentary rocks. Geology 12, 365–368.

Bojko, O., Kabała, C., 2014. Loss-on-ignition as an estimate of total organic carbon in the mountain soils. Pol. J. Soil Sci. 47, 71–79. https://doi.org/10.17951/pjss.2014.47.2.71.

Brill, D., May, S.M., Engel, M., Reyes, M., Pint, A., Opitz, S., Dierick, M., Gonzalo, L.A., Esser, S., Brückner, H., 2016. Typhoon 'aiyan's sedimentary record in coastal environments of the Philippines and its palaeotempestological implications. Nat. Hazards Earth Syst. Sci. 16, 2799–2822.

Bronk Ramsey, C., 2008. Deposition models for chronological records. Quat. Sci. Rev. 27, 42–60.

Bronk Ramsey, C., 2017. Methods for summarizing radiocarbon datasets. Radiocarbon 59, 1809–1833.

Chagué, C., Cope, J., Kilroy, C., Jacobsen, G., Zawadzki, A., Wong, H., 2020. A 7300 year record of environmental changes in a coastal wetland (Moawhitu), New Zealand, and evidence for catastrophic overwash (tsunami?). Sediment. Geol. 407, 105746 https://doi.org/10.1016/j.sedgeo.2020.105746.

Chen, X.-Y., Blockley, S.P.E., Staff, R.A., Xu, Y.-G., Menzies, M.A., 2022. Improved age estimates for Holocene Ko-g and Ma-f~j tephras in northern Japan using Bayesian statistical modelling. Quat. Geochronol. 67, 101229 https://doi.org/10.1016/j.quageo.2021.101229.

Chiba, T., Sawai, Y., 2014. Reexamination and updating of diatom species for paleoenvironmental reconstructions. Diatom 30, 17–30 (in Japanese, with English abstract).

Chiba, T., Nishimura, Y., Ohtsuka, T., 2018. Fossil diatom assemblages during the last millennium in the Toberi River mouth area, Hokkaido, Japan. Diatom 34, 8–29.

Chiba, T., Nishimura, Y., Yanagisawa, Y., 2021. Distinguishing reworked diatoms derived from Neogene marine strata in modern coastal assemblages for understanding taphonomic processes and reconstructing Holocene paleoenvironments in the Tokachi coastal area, Hokkaido, Japan. Mar. Micropaleontol., 101970 https://doi.org/10.1016/j.marmicro.2021.101970.

Dam, H., Mertens, A., Sinkeldam, J., 1994. A coded checklist and ecological indicator values of freshwater diatoms from The Netherlands. Neth. J. Aquat. Ecol. 28, 117–133.

Denys, L., 1991. A check-list of the diatoms in the Holocene deposits of the western Belgian coastal plain with a survey of their apparent ecological requirements. I. Introduction, ecological code and complete list. Belg. Geol. Dienst, Prof. Paper 246, 1–41.

Dura, T., Rubin, C.M., Kelsey, H.M., Horton, B.P., Hawkes, A., Vane, C.H., Daryono, M., Pre, C.G., Ladinsky, T., Bradley, S., 2011. Stratigraphic record of Holocene coseismic subsidence, padang, west Sumatra. J. Geophys. Res. 116, B11306 https://doi.org/10.1029/2011JB008205.

Dura, T., Cisternas, M., Horton, B.P., Ely, L.L., Nelson, A.R., Wesson, R.L., Pilarczyk, J.E., 2015. Coastal evidence for Holocene subduction-zone earthquakes and tsunamis in central Chile. Quat. Sci. Rev. 113, 93–111. https://doi.org/10.1016/j.quascirev.2014.10.015.

Dura, T., Engelhart, S.E., Vacchi, M., Horton, B.P., Kopp, R.E., Peltier, W.R., Bradley, S., 2016. The role of Holocene relative Sea-Level change in preserving records of subduction zone earthquakes. Curr. Clim. Change Rep. 2, 86–100. https://doi.org/10.1007/s40641-016-0041-y.

Dura, T., Garner, A.J., Weiss, R., Kopp, R.E., Engelhart, S.E., Witter, R.C., Briggs, R.W., Mueller, C.S., Nelson, A.R., Horton, B.P., 2021. Changing impacts of Alaska-Aleutian subduction zone tsunamis in California under future sea-level rise. Nat. Commun. 12, 1–9. https://doi.org/10.1038/s41467-021-27445-8.

Fujiwara, O., Ono, E., Yata, T., Umitsu, M., Sato, Y., Heyvaert, V.M.A., 2013. Assessing the impact of 1498 Meio earthquake and tsunami along the Enshu-nada coast, central Japan using coastal geology. Quat. Int. 308–309, 4–12. https://doi.org/10.1016/j.quaint.2012.12.009.

Fujiwara, O., Aoshima, A., Irizuki, T., Ono, E., Obrochta, S.P., Sampei, Y., Sato, Y., Takahashi, A., 2020. Tsunami deposits refine great earthquake rupture extent and recurrence over the past 1300 years along the Nankai and Tokai fault segments of the Nankai Trough, Japan. Quat. Sci. Rev. 227, 105999 https://doi.org/10.1016/j.quascirev.2019.105999.

Fujiwara, O., Irizuki, T., Obrochta, S.P., Sampei, Y., Tomotsuka, A., Haruki, A., 2022. Occurrence mode of Holocene tsunami overwash controlled by the geomorphic development along the eastern Nankai Trough, central Japan. Quat. Sci. Rev. 292, 107639 https://doi.org/10.1016/j.quascirev.2022.107639.

Furukawa, R., Nanayama, F., 2006. Holocene pyroclastic fall deposits along the Pacific coastal region of eastern Hokkaido. Bull. Volcanol. Soc. Jpn. 51, 351e371 (in Japanese, with English abstract).

Hay, R.L., Sheppard, R.A., 2001. Occurrence of zeolites in sedimentary rocks: an overview. Rev. Mineral. Geochem. 45, 217–234. https://doi.org/10.2138/rmg.2001.45.6.

Ioki, K., Tanioka, Y., 2016. Re-estimated fault model of the 17th century great earthquake off Hokkaido using tsunami deposit data. Earth Planet Sci. Lett. 433, 133–138. https://doi.org/10.1016/j.epsl.2015.10.009.

Ishizawa, T., Goto, K., Yokoyama, Y., Miyairi, Y., Sawada, C., Nishimura, Y., Sugawara, D., 2017. Sequential radiocarbon measurement of bulk peat for high-precision dating of tsunami deposits. Quat. Geochronol. 41, 202–210. https://doi.org/10.1016/j.quageo.2017.05.003.

Kato, T., 1983. Secular and earthquake-related vertical crustal movements in Japan from tidal records (1951-1981). Tectonophysics 97, 183–200.

Kelsey, H.M., Engelhart, S.E., Pilarczyk, J.E., Horton, B.P., Rubin, C.M., Daryono, M.R., Ismail, N., Hawkes, A.D., Bernhardt, C.E., Cahill, N., 2015. Accommodation space, relative sea level, and the archiving of paleo-earthquakes along subduction zones. Geology 43, 675–678. https://doi.org/10.1130/G36706.1.

Kihara, Y., Tsuda, K., Ishii, C., Ishizumi, E., Ohtsuka, T., 2015. Periphytic diatoms of Nakaikemi Wetland, an ancient peaty low moor in central Japan. Diatom 31, 18–44.

Koike, K., Machida, H., 2001. Atlas of Quaternary Marine Terraces in the Japanese Islands. Tokyo (in Japanese).

Krammer, K., Lange-Bertalot, H., Heynig, H., 1986. Bacillariophyceae 2/1. Naviculaceae. In: Ettl, H., Gerloff, J., Mollenhauser (Eds.), Süsswasserflora von Mitteleuropa. Gustav Fischer Verlag, Stuttgart, pp. 1–876.

Krammer, K., Lange-Bertalot, H., 1988. Bacillariophyceae 2/2. Basillariaceae, Epithemiaceae, Surirellaceae. In: Ettl, H., Gerloff, J., Heynig, H., Mollenhauser (Eds.), Süsswasserflora von Mitteleuropa. Gustav Fischer Verlag, Stuttgart, pp. 1–600.

Krammer, K., Lange-Bertalot, H., 1991a. Bacillariophyceae 2/3. Centrales, Fragilariaceae, Eunotiaceae. In: Ettl, H., Gerloff, J., Heynig, H., Mollenhauser (Eds.), Süsswasserflora von Mitteleuropa. Gustav Fischer Verlag, Stuttgart, pp. 1–600.

Krammer, K., Lange-Bertalot, H., 1991b. Bacillariophyceae 2/4. Achnanthaceae, Kritische Erganzungen zu Navicula (Lineolatae) und Gomphonema. In: Ettl, H. (Ed.), Pascher's Süsswasserflora von Mitteleuropa, vol2, part 4. Gustav Fischer Verlag, Stuttgart, pp. 1–437.

Leorri, E., Martin, R.E., Horton, B.P., 2009. Field experiments on bioturbation in salt marshes (Bombay Hook National Wildlife Refuge, Smyrna, DE, USA): implications for sea-level studies. J. Quat. Sci. 24, 139–149. https://doi.org/10.1002/jqs.1183.

Ludikova, A.V., Shatalova, A.E., Subetto, D.A., Kublitskiy, Y.A., Rosentau, A., Hang, T., 2020. Diatom-inferred palaeolimnological changes in a small lake in the context of the Holocene Baltic Sea transgressions: a case study of Lake Goluboye, Karelian Isthmus (NW Russia). IOP Conf. Ser. Earth Environ. Sci. 438, 012014 https://doi.org/10.1088/1755-1315/438/1/012014.

Morton, R.A., Gelfenbaum, G., Jaffe, B.E., 2007. Physical criteria for distinguishing sandy tsunami and storm deposits using modern examples. Sediment. Geol. 200, 184–207. https://doi.org/10.1016/j.sedgeo.2007.01.003.

Murakami, M., Ozawa, S., 2004. Mapped vertical deformation field of Japan derived from continuous GPS measurements and its tectonic implications. J. Seismol. Soc. Jpn. 57, 209–231 (in Japanese, with English abstract).

Nakamura, Y., 2016. Stratigraphy, distribution, and petrographic properties of Holocene tephras in Hokkaido, northern Japan. Quat. Int. 397, 52–62.

Nakanishi, R., Ashi, J., 2022. Sediment transport modeling based on geological data for Holocene coastal evolution: wave source estimation of sandy layers on the coast of Hidaka, Hokkaido, Japan. J. Geophys. Res. 127, e2022JF006721 https://doi.org/10.1029/2022JF006721.

Nakanishi, R., Okamura, S., Yokoyama, Y., Miyairi, Y., Sagayama, T., Ashi, J., 2020a. Holocene tsunami, storm, and relative sea level records obtained from the southern Hidaka coast, Hokkaido, Japan. Quat. Sci. Rev. 250, 106678 https://doi.org/10.1016/j.quascirev.2020.106678.

Nakanishi, R., Ashi, J., Okamura, S., 2020b. A dataset for distribution and characteristics of Holocene pyroclastic fall deposits along the Pacific coasts in western Hokkaido, Japan. Data Brief 33, 106565. https://doi.org/10.1016/j.dib.2020.106565.

Nakanishi, R., Ashi, J., Miyairi, Y., Yokoyama, Y., 2022a. Holocene coastal evolution, past tsunamis, and extreme wave event reconstructions using sediment cores obtained from the central coast of Hidaka, Hokkaido, Japan. Mar. Geol. 443, 106663 https://doi.org/10.1016/j.margeo.2021.106663.

Nakanishi, R., Ashi, J., Miyairi, Y., Yokoyama, Y., 2022b. Spatial extent of the mid- to late Holocene sedimentary record of tsunamis along the Southern Kuril Trench, Hokkaido, Japan. G-cubed 23, e2022GC010334. https://doi.org/10.1029/2022GC010334.

Nanayama, F., Satake, K., Furukawa, R., Shimokawa, K., Atwater, B.F., Shigeno, K., Yamaki, S., 2003. Unusually large earthquakes inferred from tsunami deposits along the Kuril trench. Nature 424, 660–663. https://doi.org/10.1038/nature01864.

Nelson, A.R., 2015. Coastal sediments. In: Shennan, I., Long, A.J., Horton, B.P. (Eds.), Handbook of Sea-Level Research. John Wiley and Sons, West Sussex, UK, pp. 47–65.

Okuno, M., Yoshimoto, M., Arai, K., Nakamura, T., Ui, T., Wada, K., 1999. AMS radiocarbon age of the Ko-f tephra from Hokkaido-Komagatake volcano, southwestern Hokkaido, Japan. J. Geol. Soc. Japan 105, 364e369 (in Japanese, with English abstract).

Okuno, J., Nakada, M., Ishii, M., Miura, H., 2014. Vertical tectonic crustal movements along the Japanese coastlines inferred from late Quaternary and recent relative sea-level changes. Quat. Sci. Rev. 91, 42–61.

Reimer, P.J., Austin, W.E.N., Bard, E., Bayliss, A., Blackwell, P.G., Ramsey, C.B., Butzin, M., Cheng, H., Edwards, R.L., Friedrich, M., Grootes, P.M., Guilderson, T.P., Hajdas, I., Heaton, T.J., Hogg, A.G., Hughen, K.A., Kromer, B., Manning, S.W., Muscheler, R., Palmer, J.G., Pearson, C., Plicht, J. van der, Reimer, R.W., Richards, D.A., Scott, E.M., Southon, J.R., Turney, C.S.M., Wacker, L., Adolphi, F., Büntgen, U., Capano, M., Fahrni, S.M., Fogtmann-Schulz, A., Friedrich, R., Köhler, P., Kudsk, S., Miyake, F., Olsen, J., Reinig, F., Sakamoto, M., Sookdeo, A., Talamo, S., 2020. The IntCal20 northern hemisphere radiocarbon age calibration curve (0–55 cal kBP). Radiocarbon 62, 725–757. https://doi.org/10.1017/RDC.2020.41.

Richmond, B., Szczuciński, W., Chagué-Goff, C., Goto, K., Sugawara, D., Witter, R., Tappin, D.R., Jaffe, B., Fujino, S., Nishimura, Y., Goff, J., 2012. Erosion, deposition and landscape change on the Sendai coastal plain, Japan, resulting from the March 11, 2011 Tohoku-oki tsunami. Sediment. Geol. 282, 27–39. https://doi.org/10.1016/j.sedgeo.2012.08.005.

Sagayama, T., Hoyanagi, K., Miyasaka, S., 1992. Diatom biostratigraphy and the stage of Neogene coarse-grained deposits in the Hidaka coastal land, central Hokkaido, Japan.Jour. Geol. Soc. Japan 98, 309–321 (in Japanese with English abstract).

Satake, K., 2015. Geological and historical evidence of irregular recurrent earthquakes in Japan. Philos. Trans. R. Soc. A-Math. Phys. Eng. Sci. 373, 20140375 https://doi.org/10.1098/rsta.2014.0375.

Sato, H., 2001. Holocene uplift derived from relative sea-level records along the coast of western Kobe, Japan. Quat. Sci. Rev. 20, 1459–1474. https://doi.org/10.1016/S0277-3791(01)00005-1.

Sato, H., 2002. Late Holocene diatom assemblages and sea-level observation at a site in Okayama City along the northeastern coast of the Seto Inland Sea. Nat. Hum. Activit. 7, 27–33.

Sato, H., Maeda, Y., Kumano, S., 1983. Diatom assemblages and Holocene sea level changes at the Tamatsu site in Kobe, western Japan. Quat. Res. 22, 77–90. https://doi.org/10.4116/jaqua.22.77.

Sawai, Y., Nagumo, T., 2003. Diatom (Bacillariophyceae) flora of salt marshes along the Pacific coast of eastern Hokkaido, northern Japan. Bull. Nippon Dent. Univ. Gen. Educ. 32, 93–108.

Sawai, Y., Horton, B.P., Nagumo, T., 2004a. Diatom–based elevation transfer function along the Pacific coast of eastern Hokkadio, northern Japan—an aid in paleo-seismic study along the coasts near Kurile subduction zone. Quat. Sci. Rev. 23, 2467–2483.

Sawai, Y., Satake, K., Kamataki, T., Nasu, H., Shishikura, M., Atwater, B.F., Horton, B.P., Kelsey, H.M., Nagumo, T., Yamaguchi, M., 2004b. Transient uplift after a 17th-century earthquake along the Kuril subduction zone. Science 306 (5703), 1918–1920. https://doi.org/10.1126/science.1104895.

Sawai, Y., Kamataki, T., Shishikura, M., Nasu, H., Okamura, Y., Satake, K., Thomson, K. H., Matsumoto, D., Fujii, Y., Komatsubara, J., Aung, T.T., 2009. Aperiodic recurrence of geologically recorded tsunamis during the past 5500 years in eastern Hokkaido, Japan. J. Geophys. Res. 114, B01319 https://doi.org/10.1029/2007JB005503.

Sawai, Y., Namegaya, Y., Tamura, T., Nakashima, R., Tanigawa, K., 2015. Shorter intervals between great earthquakes near Sendai: Scour ponds and a sand layer attributable to A.D. 1454 overwash. Geophys. Res. Lett. 42, 4795–4800. https://doi.org/10.1002/2015GL064167.

Sawai, Y., 2020. Subduction zone paleoseismology along the Pacific coast of northeast Japan — progress and remaining problems. Earth Sci. Rev. 208, 103261 https://doi.org/10.1016/j.earscirev.2020.103261.

Scileppi, E., Donnelly, J.P., 2007. Sedimentary evidence of hurricane strikes in western Long Island, New York. G-cubed 8. https://doi.org/10.1029/2006GC001463.

Stabell, B., 1985. The development and succession of taxa within the diatom genus Fragilaria Lyngbye as a response to basin isolation from the sea. Boreas 14, 273–286. https://doi.org/10.1111/j.1502-3885.1985.tb00916.x.

Spiske, M., Piepenbreier, J., Benavente, C., Bahlburg, H., 2013. Preservation potential of tsunami deposits on arid siliciclastic coasts. Earth Sci. Rev. 126, 58–73. https://doi.org/10.1016/j.earscirev.2013.07.009.

Takada, K., Nakata, T., Miyagi, T., Haraguchi, T., Nishitani, Y., 2002. Handy Geoslicer—new soil sampler for Quaternary geologist. Chishitsu News 579, 12–18 (in Japanese).

Takashimizu, Y., Urabe, A., Suzuki, K., Sato, Y., 2012. Deposition by the 2011 Tohoku-oki tsunami on coastal lowland controlled by beach ridges near Sendai, Japan. Sediment. Geol. 282, 124–141. https://doi.org/10.1016/j.sedgeo.2012.07.004.

Tröels-Smith, J., 1955. Characterization of Unconsolidated Sediments. Geological Survey of Denmark, Series IV. No. 10.

Vos, P.C., de Wolf, H., 1993. Diatoms as a tool for reconstruction sedimentary environments in coastal wetlands: methodological aspects. Hydrobiologia 269/270, 285–296.

Wada, N., Takahashi, K., Watanabe, J., Kanie, Y., 1992. Explanatory Text of the Geological Map of Japan, Scale 1:50,000, "Mitsuishi.". Geological Survey of Japan, pp. 1–78 (in Japanese with English abstract).

Watanabe, T., Ohtsuka, T., Tuji, A., Houki, A., 2005. Picture Bookand Ecology of the Freshwater Diatoms. Uchida Rokakuho Publishing Company, Tokyo (in Japanese).

Wheatcroft, R.A., 1990. Preservation potential of sedimentary event layers. Geology 18, 843–845. https://doi.org/10.1130/0091-7613(1990)018<0843:PPOSEL>2.3.CO;2.

Witkowski, A., Lange-Bertalot, H., Metzeltin, D., 2000. Diatom flora of marine coasts 1. In: Lange-Bertalot, H. (Ed.), Iconographia Diatomologica 7. Koeltz Scientific Books, Königstein.

Woodward, C.A., Gadd, P.S., 2019. The potential power and pitfalls of using the X-ray fluorescence molybdenum incoherent: coherent scattering ratio as a proxy for sediment organic content. Quat. Int. 514, 30–43. https://doi.org/10.1016/j.quaint.2018.11.031.

Yanai, S., Igarashi, Y., 1990. History of the slope failure and paleoenvironment on the marine terrace of Hidaka district, central Hokkaido. Quat. Res. 29, 319–336 (in Japanese with English abstract).

Yokoyama, Y., Purcell, A., 2021. On the geophysical processes impacting palaeo-sea-level observations. Geosci. Lett. 8, 13. https://doi.org/10.1186/s40562-021-00184-w.

Yokoyama, Y., Miyairi, Y., Matsuzaki, H., Tsunomori, F., 2007. Relation between acid dissolution time in the vacuum test tube and time required for graphitization for AMS target preparation. Nucl. Instrum. Methods Phys. Res. 259, 330–334.

Yokoyama, Y., Okuno, J., Miyairi, Y., 2012. Holocene sea-level change and Antarctic melting history derivedf from geological observations and geophysical modeling along the Shimokita Peninsula, northern Japan. Geophys. Res. Lett. 39, L13502 https://doi.org/10.1029/2012GL051983.

Yokoyama, Y., Hirabayashi, S., Goto, K., Okuno, J., Sproson, A.D., Haraguchi, T., Ratnayake, N., Miyairi, Y., 2019a. Holocene Indian Ocean sea level, Antarctic melting history and past Tsunami deposits inferred using sea level reconstructions from the Sri Lankan, Southeastern Indian and Maldivian coasts. Quat. Sci. Rev. 206, 150–161. https://doi.org/10.1016/j.quascirev.2018.11.024.

Yokoyama, Y., Miyairi, Y., Aze, T., Yamane, M., Sawada, C., Ando, Y., de Natris, M., Hirabayashi, S., Ishiwa, T., Sato, N., Fukuyo, N., 2019b. A single stage accelerator mass spectrometry at the atmosphere and Ocean Research Institute, the university of Tokyo. Nucl. Instrum. Methods Phys. Res., Sect. B 455, 311–316. https://doi.org/10.1016/j.nimb.2019.01.055.

Zong, Y., Sawai, Y., 2015. Diatoms. In: Shennan, I., Long, A.J., Horton, B.P. (Eds.), Handbook of Sea-Level Research. John Wiley and Sons, West Sussex, UK, pp. 233–248.